

**Contribution of Climate Change to the  
Risk of Intensifying Storms and Monetary  
Losses in New York City**

**Prepared by:** Ali Sarhadi

**Supervised by:** Kerry Emanuel

**Date:** April 2, 2023

# Contents

<b>1</b>	<b>Overview</b>	<b>1</b>
<b>2</b>	<b>Risk Assessment of Compound Flooding from tropical and extratropical cyclones</b>	<b>2</b>
2.1	Compound flooding effect . . . . .	3
2.2	Sandy’s compound flooding . . . . .	5
2.3	Tropical Cyclones compound flooding risk in today’s climate . . . . .	6
2.4	Future Compound flooding risk . . . . .	8
2.5	Compound flooding risk of ETCs . . . . .	10
2.6	Discussion . . . . .	13
<b>3</b>	<b>Risk Assessment of Wind-Driven Damage from hurricanes</b>	<b>15</b>
3.1	Downscaling of hurricanes and their corresponding wind events . . . . .	15
3.2	Optimizing damage function using conditional random field theory . . . . .	15
3.3	Quantifying the risk of monetary losses from intensifying storms in current and future climates . . . . .	19
3.4	Discussion . . . . .	21
<b>4</b>	<b>Publications supported under this contract</b>	<b>22</b>
<b>A</b>	<b>Appendix</b>	<b>27</b>

# 1 Overview

Tropical Cyclones (TCs) and Extratropical Cyclones (ETCs) cause significant monetary losses in the eastern part of the United States every year. The effect of anthropogenic warming on these storms has led to changes in the risk and damages associated with them in recent decades, and it is expected to intensify in the future. This research aims to develop a physics-based methodology to better understand the extent to which climate change has altered and will change the risk of multiple hazards associated with these storms, including compound surge and rainfall-driven flooding and high-speed surface winds.

The first section of the research focuses on developing a physics-based methodology to quantify the risk of compound flooding from TCs and ETCs in current and future decades in New York City (NYC). Due to the limited availability of instrumental hurricane records in NYC, a physics-based statistical-deterministic downscaling approach is used to estimate the climatology and evolution of hurricanes under both current and future climates. A high-resolution statistical-deterministic tropical cyclone model is employed, which uses time-evolving boundary conditions derived from the output data of General Circulation Models (GCMs) to downscale synthetic hurricanes. By generating a large set of synthetic hurricanes that are consistent with the ERA-Interim reanalysis and GCM climates, the climatology and evolution of hurricanes in NYC are estimated. The research also uses dynamically downscaled extratropical cyclones and their main drivers to simulate compound flooding. Using hydrodynamic models forced by large sets of synthetic TCs from four Coupled Model Intercomparison Project Phase 6 (CMIP6) climate models and ETC events downscaled using Weather Research and Forecasting (WRF) model forced by CMIP5 simulations, the contribution of the primary drivers to increasing risk of spatially-varying compound flooding is quantified in current and future warming decades in NYC.

The second section of the research uses the same physics-based model to simulate high spatial resolution maximum wind speed during the landfalling of historical hurricanes. A computational intelligence model is developed using conditional random field theory to optimize wind-driven damage functions in grid cells with the size of 5 in 5 km in NYC. By applying these optimized wind-driven damage functions on future synthetic hurricanes' maximum wind speed, the monetary losses from maximum sustained wind of hurricanes are projected in the future warming climate. By using a probabilistic model, the risk of monetary losses from hurricanes' wind speed in the future warming climate is quantified to the portfolio of Homesite in the NYC area.

Overall, this research presents a physics-based methodology to better understand the risks of multiple hazards from TCs and ETCs in a warming climate. The study demonstrates that this methodology can be used to quantify the multiple hazards involved with TCs and ETCs and the associated losses caused by these storms in the current and future warming decades in NYC. Although the study does not quantify the effect of climate change on the losses arising from compound flooding, it does provide insight into the risk of monetary losses from high-speed winds of these storms. As an insurance company, Homesite can use these results to better project the potential impacts of TCs and ETCs in a warming climate to develop new policies, set premiums, and respond to claims related

to these multiple hazards from these intensifying storms in a future warming climate.

## 2 Risk Assessment of Compound Flooding from tropical and extratropical cyclones

TCs and ETCs are among the deadliest and most destructive natural hazards, causing substantial fatalities and economic damages (US\$26 billion from TCs and US\$2 billion from winter ETCs each year in the United-States alone) [1, 2]. Among multiple hazards associated with these cyclones, many of the fatalities and much of the damage are caused by coastal flooding from storm surge (generated by high-speed winds), and inland flooding rain-driven in coastal and inland communities [3, 4]. During destructive cyclones, each of these flooding hazards may play a role, either separately or in combination. For example, strong winds during Hurricane Sandy in October 2012 caused devastating surge-driven flooding across heavily populated coastal areas in New York City (NYC), resulting in more than \$64 billion (2017 USD) in damages [5]. Hurricane Harvey in August 2017, instead, stalled over an inland area and poured an unprecedented heavy rainfall for many days over the Houston metropolitan area, causing catastrophic inland flooding and costing \$125 billion (2017 USD) in damages [3]. However, storm surge driven flooding may co-occur with inland heavy rainfall-driven flooding resulting in a compound flooding event, whose destructive potential is often much greater than that of either of the individual flooding hazards. During Hurricane Katrina, a destructive category 5 TC, a significant storm surge coincided with record-breaking heavy inland rainfall along the Gulf coast. The compound flooding devastated coastal areas in Louisiana and caused one of the costliest natural disasters in U.S. history, with at least 1,833 deaths and more than \$160 billion in damages (adjusted to 2017 USD to compare with the rainfall dominant Hurricane Harvey) [6]. Recently, a destructive compound flooding event during Hurricane Ian had devastating impact in western Florida, and cost between \$50 billion and \$65 billion in insured losses. In densely populated coastal areas, such flood hazard compounding in TCs or ETCs can thus lead to extreme impacts even if, individually, these flooding hazards are not extreme [7].

Past and future changes in the risk of compound flooding from these cyclones depend on how the warming atmosphere and oceans have influenced and will influence the structural characteristics, intensity, frequency, and movement of these cyclones [8]. There is confidence that anthropogenic warming has intensified the activity and destructiveness of major TCs in the North Atlantic basin in recent decades [9, 10, 11, 12]. This trend is expected to accelerate in the future as ocean temperatures increase [13, 14, 10, 15], and the troposphere warms [6, 8, 16, 17]. Despite our understanding of the future changes of multiple individual drivers of TC and ETC flooding under a warming climate—including intensifying rainfall, poleward migration, slowdown of cyclone translation speed, Sea Level Rise (SLR), and deceleration of ETCs due to atmospheric blocking [8, 18, 19, 5]—quantifying the risk of compound flooding in response to these changes in highly populated coastal cities, like NYC, remains elusive.

In recent years, much effort has been devoted to modeling the complex hydrodynamics of compound flooding from TCs and ETCs and their corresponding risk in highly populated coastal areas. The majority of these studies model risk statistically, based on individual

predictors such as surge height and rainfall intensity verified using local observations [20, 7]. Recent studies have introduced physically based computational models to supplement statistical risk assessment approaches [21, 22, 23, 24, 25, 26, 27]. Most of these have been used to predict rainfall, not flooding, or focus on surge-only flooding. In this study, we introduce a physically based computational approach to model compound flooding and address how human-induced climate change and SLR may affect flooding and flood risk in NYC from TCs and ETCs.

First, we estimate the climatology and evolution of TCs in the current and future climates by using a physics-based statistical-deterministic downscaling approach [28]. This method generates a large number of synthetic TCs consistent with the ERA-Interim reanalysis and General Circulation Model (GCM) climates to emulate a long record of historical and future TC events. We downscale a large set of storms from ERA-Interim reanalysis from the late 20th century (1979-1999), and the early 21st century (2000-2020) climates. We also downscale a large set of synthetic tracks from four bias corrected GCMs of the Coupled Model Intercomparison Project phase 6 (CMIP6), to represent the evolution of TCs in the current climate (2000-2014), and at the middle (2041-2060) and end of the century (2081-2100) under the SSP3 7.0 scenario. The Tropical Cyclone Rainfall (TCR) algorithm is used to estimate evolving, high spatial resolution (almost  $\sim 20$  m) hourly rainfall from the synthetic TCs in and near NYC [29]. Second, for ETC events, we use a dynamically downscaled dataset of hourly rainfall, wind, and pressure fields over the Northeastern U.S., with 3-km spatial resolution, driven by CESM v1.0 under Representative Concentration Pathway 8.5 (RCP8.5). The downscaling data comes from convection-permitting Weather Research and Forecasting (WRF) model simulations for almost the same three climate periods [30]. We then use an extensively evaluated hydrodynamic model (GeoCLAW) driven by atmospheric pressure and surface wind speed to compute surge height associated with TCs and ETCs, along a vast segment of coastline near NYC [31]. The hydrodynamic model also accounts for SLR from the ensemble mean of CMIP6 projections, incorporated to the model as a ‘bathtub’ approach (see more details on the data sets in Appendix). We then apply a pluvial hydraulic model [32], driven by the simulated storm surges and downscaled heavy rainfall events simultaneously as boundary conditions. The hydraulic model then simulates high spatio-temporal resolution compound flooding during the landfalling of each synthetic TC and downscaled ETC in the current and future climates (see more details in Appendix). Finally, we quantify the extent to which changes in storm climatology and SLR from anthropogenic forcing may change the spatial risk of compound flooding events in NYC.

## 2.1 Compound flooding effect

Figure 1 (A-D) compares the behavior of compound flooding with the individual surge and rainfall driven flooding in different locations in NYC (coastal and inland areas), based on the simulations from a randomly selected synthetic track in the current climate in NYC. The combination of the individual surge and rainfall driven flooding is nonlinear (Figure 1 (B-D)). This nonlinear effect depends on different factors, including the nature of the storm (whether it is wind or rainfall dominant), topography and the distance from coastline, and the lag time between surge and rainfall driven flooding. Although the contribution of surge driven flooding dominates in coastal areas, in inland areas rainfall driven flooding is the dominant factor. In both coastal and inland areas, however, the

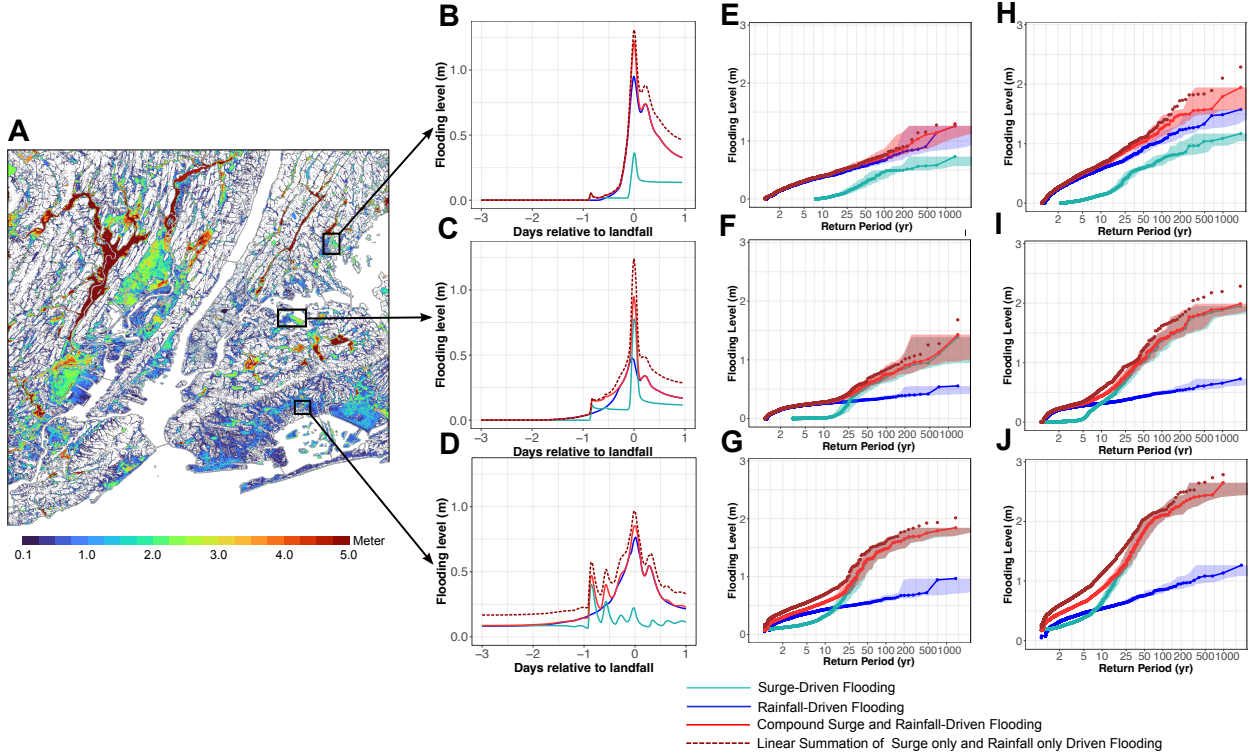


Figure 1: (A) Maximum compound flooding level for a downscaled synthetic track (#260) from CESM2 model under the current climate. (B-D) Compounding effect from nonlinear mechanical interaction between surge and rainfall driven flooding through landfalling the synthetic TC in the three depicted areas in NYC. (E-G) Flooding levels as a function of return period from the three flooding hazard sources. The results are based on synthetic TCs generated from CESM2 model over the current climate (the results are calculated based on the mean of flooding levels for each depicted area). The shading part in the figure represents sampling uncertainty bounds calculated based on the 5th and 95th percentiles of a Poisson distribution (H-J) Similar to the previous section, but for the end of the century.

compound flooding levels are higher than the individual hazards at the time of landfalling. We also show that a linear summation of the individual surge and rainfall-driven flooding (red dashed line) cannot represent the level of compound flooding. Summing the two individual flooding levels overestimates the level of ‘actual’ compound flooding.

This effect of compounding will also affect risk assessments in the current and future warming climate. In assessing TC flood risk, different studies typically consider the risk of one individual hazard [24, 33, 22] and may use statistical algorithms to account for other hazard components [27, 26]. These approaches, however, ignore the spatiotemporal nonlinear mechanical interactions between the surge and rainfall driven flooding, which can lead to higher potential for compound flooding across the coastal and inland areas. For example, Figure 1 (E) shows that relying on only surge driven flooding in inland areas underestimates the risk of actual compound flooding up to 62.6% (51.0-61.6%) in the current climate, and up to 59.0% (55.8-56.5%) in the late 21st century for the events which occur once in 100 y (Figure 1 (H)). In coastal areas, however, relying on only rainfall driven flooding underestimates the risk of compound flooding by up to 40.0% (41.8-42.2%) in the current climate, and by up to 40.6% (39.3-41.7%) in the late 21st century for the same events (Figure 1 (G and J)). On the other hand, the linear

summation of the individual surge and rainfall-driven flooding overestimates the risk of flooding, comparing to the actual compound flooding. This misestimation of the risk occurs more from the low frequency events in the upper tail in both current and future climates. Therefore, accounting for the spatiotemporal nonlinear compound effects of surge and rainfall driven flooding during landfalling and their responses in coastal and inland areas is crucial in assessing coastal flooding risk.

## 2.2 Sandy’s compound flooding

We begin by looking at a single TC event, one that resembles Hurricane Sandy, which affected NYC in 2012. In addition to constructing a map of the flooding, we examine the individual and combined contributions of rainfall and surge to the flooding. Figure 2 summarizes this particular event, showing the maximum wind speed experienced at each point during the event (A), and the accumulated hourly rainfall from this event (B). Figures 2 (C) and (D) show, respectively, the maximum surge height, and rainfall-driven flooding from this event, while Figure 2 (E) shows the compound flooding driven by both sources. This simulated maximum compound flooding from the Sandy-like synthetic event is similar to the actual Federal Emergency Management Agency (FEMA) flood inundation record from Sandy in 2012 (Figure S1). Figure 2 (C-E) shows that the individual rainfall and surge hazards, as well as the compound hazard, may affect different areas. Figure 2 (F) also shows under-estimation of the property value exposure under different levels of flooding from the individual hazards comparing to the one from compound flooding during Hurricane Sandy. It is clear that accounting only for individual flooding hazards mis-estimates the magnitude, damage, and spatial consequences of flooding relative to compound flooding. In addition, the spatial information provided by our physics-based model, which identified the most at-risk zones, is crucial for adaptation measures and cannot be well simulated using statistical methods alone.

## 2.3 Tropical Cyclones compound flooding risk in today's climate

Next, we quantify the extent to which anthropogenic warming has already changed the risk of compound flooding via changes in TC climatology and SLR in and near NYC. To do so, we simulate the maximum compound flooding level from 1250 synthetic TCs downscaled from ERA-Interim reanalysis under the late 20th century climate, and another 1250 events in the climate of the early 21st century. Figure 3 (A) shows the changes in the risk of compound flooding between the late 20th century and the early 21st century. The return period is calculated as the inverse of the annual exceedance probability defined over each of the two time periods. The results show that anthropogenic warming already has increased significantly the risk for events with return periods between 2 and 20 *yr* in today's climate for the selected area. Sampling uncertainty prevents us from distinguishing trends at larger return periods.

Figure 3 (B) shows that climate change has increased the spatial risk of compound flooding by 100 *yr* return period events. The flood levels of such events have increased in inland areas by up to  $\sim 0.5$  *m*, caused mostly by more intense rainfall. However, there is a decreasing trend along the coastlines up to  $\sim -0.2$  *m*. This decrease might be related to the decrease in the frequency or changes in tracks of intense TCs in the region, which generate lower surge height and compound flooding along the coastlines for such events in the more recent climate. A comparison of figure 3 to Figure S2, which neglects SLR, also confirms that SLR does not appear to have contributed significantly to the change in compound risk in recent years. The compound flooding results for events with return periods 25 to 500 *yr* are provided in Figures S3. The risk of compound flooding, especially for the low frequency events, follows a pattern similar to that of the 100 *yr* return period shown in Figure 3 (B), and the changes are not statistically significant in coastal areas.

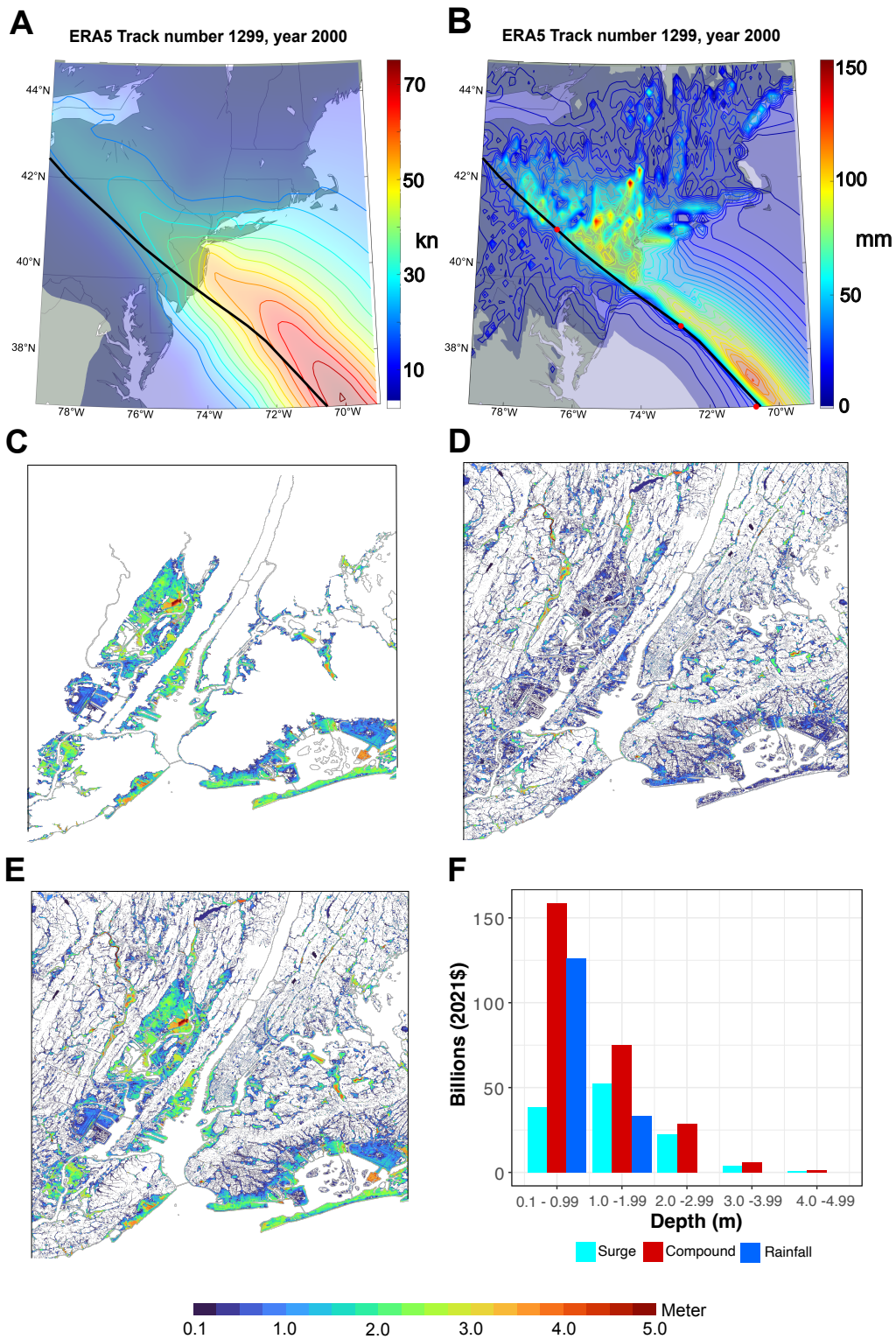


Figure 2: (A) Max. wind speed swath of a Sandy-like synthetic track (#1299) downscaled from ERA5. (B) Same as (A) but for rainfall intensity. (C) Surge driven flooding for the Sandy-like event (#1299), (D) Rainfall driven flooding for the Sandy-like event (#1299), (E) Compound surge and rainfall driven flooding for the Sandy-like event (#1299). (F) Property value exposure to different levels of flooding from each flooding hazard during Hurricane Sandy in NYC.

## 2.4 Future Compound flooding risk

By simulating compound flooding levels from a large set of synthetic TCs downscaled from the four climate models (i.e., CESM2, CNRM6, ECEARTH6, and UKMO6) for the current and future climates, we quantify how the risk of compound flooding may evolve. Figure 4 (A and B) shows the respective contributions to compound flooding risk intensification arising from storm climatology changes and SLR. Each curve represents the simulated TC compound flooding events generated from each of the four CMIP6 models. Based on the results, the return period of the Sandy-like event (depicted in dash-line) is about  $\sim 215$  *yr* based on the ensemble mean of the four CMIP6 climate models neglecting SLR in the current climate. Going forward in time while still neglecting changes in SLR, the return period of Sandy-like events decreases to  $\sim 170$  *yr* by the middle of the century, and to  $\sim 130$  *yr* by the end of the century. With the joint effect of changes in TC climatology and SLR, the Sandy-like event occurs around once in  $\sim 150$  *yr* in the present climate. The risk of such a damaging event will also increase and become a  $\sim 65$  *yr* event by the middle of the century, and a  $\sim 30$  *yr* storm by the end of the century. TC climatology changes arising from anthropogenic warming alone will thus increase the risk of a Sandy-like storm by up to 1.26 times by the middle of the century and 1.7 times by the end of the century, relative to the current climate. The joint contribution of TC climatology and SLR will, however, increase the risk of Sandy-like floods by up to almost 2.3 times by the middle of the century, and 5 times by the end of the century. The projected SLR alone will intensify the risk of Sandy's compound flooding by 1.05 times by the middle of the century and 3.3 times by the end of the century relative to the current climate. SLR thus makes a significant contribution to the increased risk of destructive compound flooding events from TCs.

Figure 4 (C-F) shows the contribution of each primary driver to the change in 100 *yr* flooding by the middle and end of the century. The results show that, by the middle of the century, anthropogenic warming will intensify the level of spatial flooding, mostly in inland areas and arising mostly from increased rainfall. A comparison between Figure 4 (C) and (D) shows the contribution of SLR to changes in compound flooding by the mid-century. For example, TC climatology change increases the spatial compound flooding level, on average, up to  $\sim 0.35$  *m*, while the joint contribution of TC changes and SLR will increase flood levels by up to  $\sim 0.7$  *m* in coastal areas.

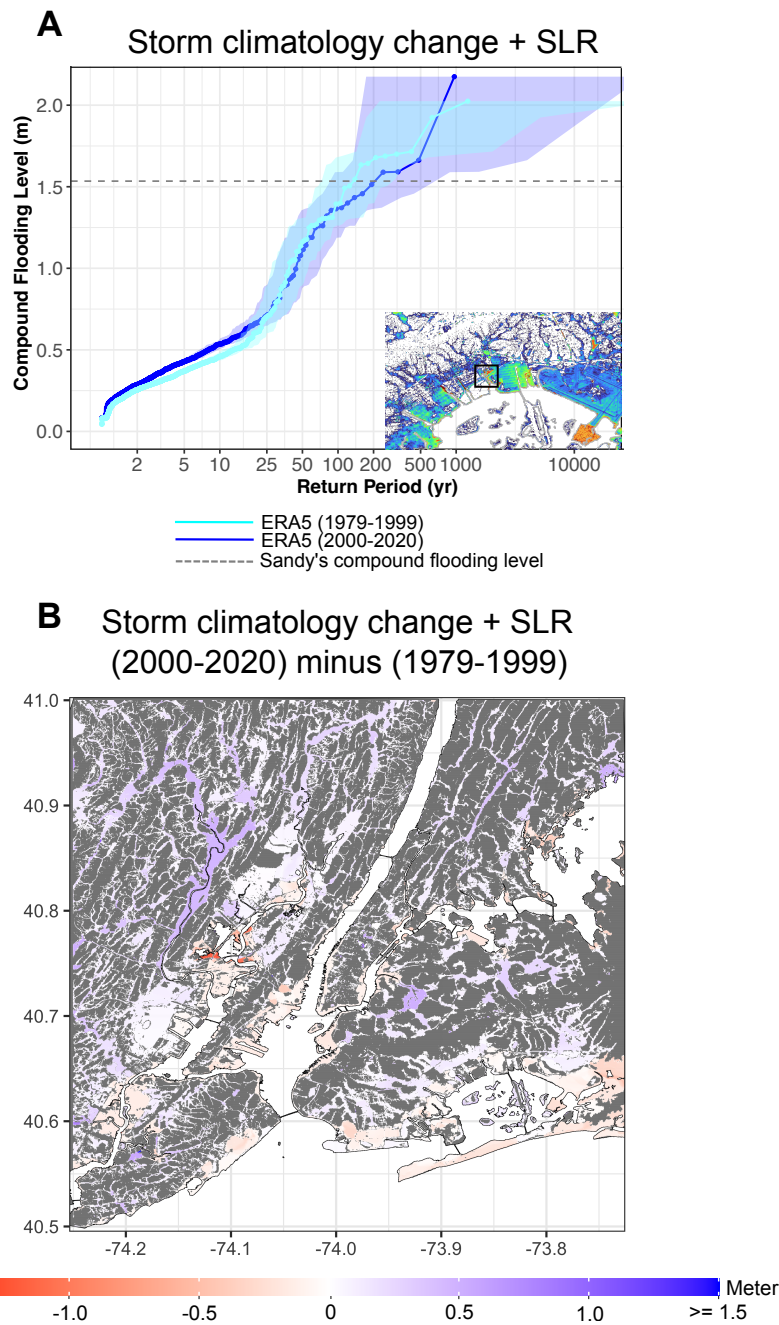


Figure 3: Impact of TC climatology change and SLR on the risk of compound flooding in today's climate (2000-2020) relative to the end of the 20<sup>th</sup> century (1979-1999) in NYC. (A) TC compound flooding level as a function of return period, for today's climate and the end of the 20<sup>th</sup> century (the results are calculated based on the mean of compound flooding for the depicted area). Each line shows compound flooding results from synthetic TCs generated from re-analysis ERA5 over each time period. The shading in the figure represents sampling uncertainty bounds calculated based on the 5<sup>th</sup> and 95<sup>th</sup> percentiles of a Poisson distribution. The gray dashed line shows the mean of Sandy compound flooding level, calculated from the Sandy-like event (#1299) for the depicted area (shown in a black rectangle). (B) Impact of TC climatology change and SLR on the spatial risk of 100 *yr* return period compound flooding events in today's climate relative to the late 20<sup>th</sup> century (blue color shows increasing trend, and red color shows decreasing trend).

Similarly, TC climatology changes increase rainfall intensity by the end of century, resulting in more increased flooding in inland areas, especially along the Passaic River. This contribution alone increases the level of spatial compound flooding by up to almost  $\sim 0.5$   $m$  by the end of the century in coastal areas (Figure 4-E). The joint impact including SLR, however, increases the level of flooding on average by up to  $\sim 1.3$   $m$  in the majority of coastal areas by the end of the century (Figure 4-F). These results show the significant impact of SLR in increasing flood risk in NYC. The contributions of both drivers to increasing flood risk for other return periods from 50  $yr$  to 500  $yr$  are given in Figure S(4-6).

## 2.5 Compound flooding risk of ETCs

Figure 5 (A and B) show the contributions of ETC climatology changes and SLR to changes in compound flooding risk over the depicted area. The results cover only high frequency events (return periods of 20  $yr$  or less), due to the limited number of ETCs available in the downscaled data. With ETC climatology change only, the risk of compound flooding is projected to increase 1.7 times by the middle of the century, and 2.4 times more by the end of the century. The combined impact of ETC climatology change and SLR will, however, increase the risk by a factor of about 5.4 by the middle of the century, and about 9 by the end of the century. Considering only SLR, the risk increases by a factor of 3.7 by the middle of the century, and by 6.6 by the end of the century. In this case, SLR is more important than changes in ETC climatology change in driving increased flooding.

The impacts of ETC storm changes and SLR on the spatial risk of compound flooding for 15  $yr$  return period events are shown in Figure 5 (C and D) for the middle of the century, and in Figure 5 (E and F) for the end of the century. The results indicate the dominant role of SLR in increasing the risk of ETC-related compound flooding of coastal areas. The results for the impact of ETC climatology changes and SLR on the risk of compound flooding for other return periods (5  $yr$  to 10  $yr$ ) are shown in Figure S(7-8).

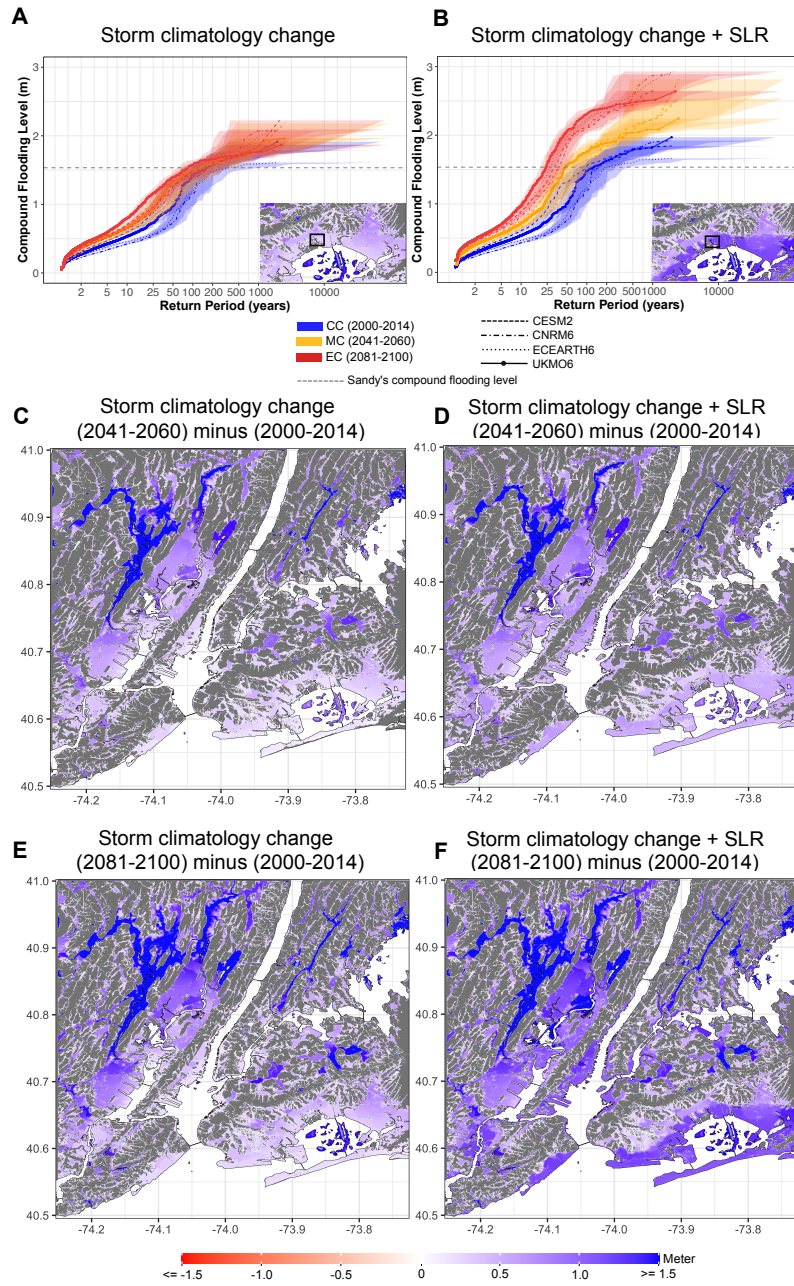


Figure 4: Impact of future TC climatology change and SLR on the risk of compound flooding in NYC. (A) Contribution of TC climatology change alone, and (B) contribution of both TC climatology change and SLR to the future risk of compound flooding. The results are based on the mean of compound flooding level (calculated for the depicted coastal area) in the current and future climates. Each line shows the results from synthetic TCs downscaled from each climate model in the current and future climates. The shading in the figure represents confidence intervals calculated based on the 5th and 95th percentiles of a Poisson distribution for each model. The gray dashed line shows the magnitude of compound flooding from Sandy (calculated from the Sandy-like event (#1299) for the depicted area. (C and D) Impact of TC climatology change and SLR on the spatial risk of 100 *yr* return period compound flooding by the middle of the century relative to the current climate, and (E and F) by the end of the century relative to the current climate. Note that the spatial results are based on the ensemble mean of the four CMIP6 climate models calculated in each climate.

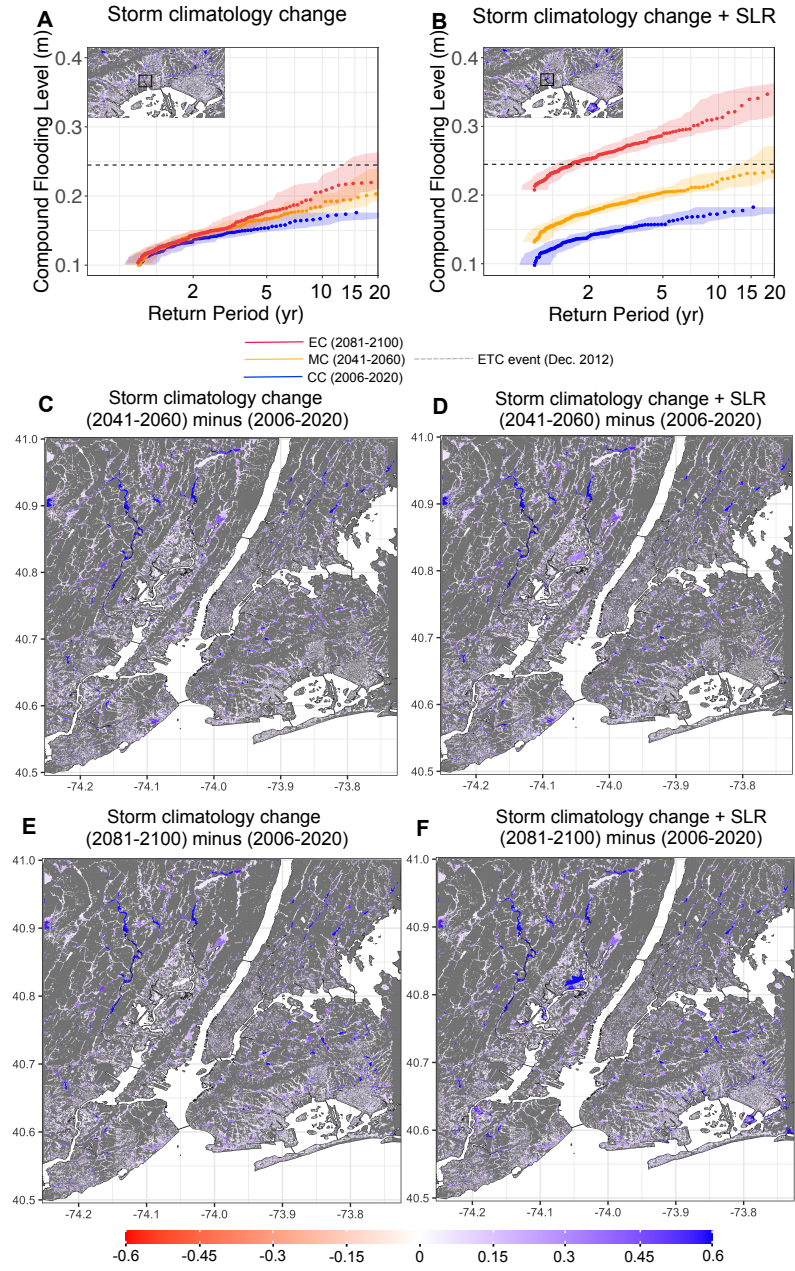


Figure 5: Impact of current and future changes in storm climatology and SLR on the risk of ETC compound flooding in NYC. (A and B) Individual and joint contribution of storm climatology changes and SLR on the risk of ETC compound flooding in the current and future climates. The results are based on the mean of compound flooding level calculated for the depicted area. Each line shows the results for ETC events dynamically downscaled by WRF in the current and future climates. The gray dashed line shows the magnitude of compound flooding from the ETC which occurred in December 2012 for the depicted area.(C and D) Impact of storm climatology changes and SLR on the spatial risk of 15 *yr* return period ETC compound flooding events by the middle of the century relative to the current climate, and ( E and F) by the end of the century relative to the current climate.

## 2.6 Discussion

In this study we demonstrated the contribution of SLR and TC and ETC climatology changes to intensifying flooding hazard in NYC. We found that anthropogenically induced changes to TC activity have already increased flood risk in NYC. This risk increase translates to more damage from upper tail events, consistent with previous studies on the effect of anthropogenic warming on the risk and damages of extreme storms [5, 21, 24]. Our findings reveal that the effect of SLR on flooding from TCs and ETCs has been underestimated, relative to the impact of storm climatology changes in previous studies [24, 33]. Most previous studies did not employ spatially-detailed hydrodynamic simulations of compound surge and rainfall driven flooding. Simpler, often statistical methods used in previous studies are not well suited to quantifying spatially and temporally varying flood risk or the contributions of the individual drivers to the net flooding. This information is essential to designing robust adaptation and mitigation measures. By ignoring the mechanical and nonlinear hydrodynamics of compound flooding, they underestimate the risk of extreme storms such as Hurricane Sandy. According to our physics-based approach, Sandy-like compound flooding occurs around once every  $\sim 150$  *yr* compared to previous estimates of  $\sim 400$ - $500$  *yr* [24, 33, 22], and will occur once every  $\sim 65$  *yr* by the middle of the century, and once every  $\sim 30$  *yr* by the end of the century under the SSP3-7.0 scenario. We believe that the current risk of compound flooding from ETCs has also been underestimated in prior studies. We thus provide evidence that the frequency and intensity of compound flooding in NYC from both TCs and ETCs could increase, with rapidly growing risk to communities and infrastructure. Our results are also consistent with the work of [26], showing that SLR is the most dominant driver of the joint rainfall-surge hazard in the future in NYC.

The approach we use to quantify TC risk is capable of assessing risks from very low frequency events, since we can generate an almost unlimited number of synthetic cyclones. By contrast, our assessment of ETC-associated risk is severely circumscribed by the low number of events one can afford to simulate with embedded, three-dimensional models like WRF. Future research should explore better and more efficient ways of downscaling extratropical cyclones. It may be that the only practical way forward is to run ensembles of high-resolution global models in present and future climates and infer ETC climatology directly from the output. This would require extraordinary resources to carry out the simulations and to analyze the resulting output. We did not include astronomical tides in our calculations; these should be included in future surge and compound flood risk assessments. Finally, our TC downscaling is not ideally suited to extratropical transitioning storms like Sandy. As such storms can be very destructive, more work needs to be done on assessing their risks and how they might evolve under climate change.

Overall, this study emphasizes how vulnerable coastal communities are and should serve as a guide to how they might assess and adapt to increasing flooding risk from tropical and extratropical cyclones. Our physics-based methodology can be easily transferred to other tropical and extratropical vulnerable coastal regions with no instrumental records to provide critical insight on the role of human-made global warming in changing the risk of TC and ETC induced compound flooding in the current and future decades. Our findings could help decision makers adapt coastal cities and infrastructure to mitigate adverse consequences arising from intensifying compound flooding risk. Human-made

climate change and SLR can be viewed as threat multipliers to the risk of compound flooding from TCs and ETCs. Along with the greenhouse gas emission reductions needed to mitigate climate change, further work that informs adaptation, such as the present study, is critical to limiting the risk and damage associated with a warming climate. It should be noted that data related to flooding damage may not always be readily available to the public, particularly with respect to quantifying the monetary losses to properties resulting from compound flooding and the anticipated damage from SLR in the current and future decades within a given study area. If a proprietary dataset containing this information were to become available, it could enable the generation of estimates for the monetary losses caused by both high and low frequency tropical and extratropical storms in both current and future climates.

### 3 Risk Assessment of Wind-Driven Damage from hurricanes

In this section, we present a model that accurately assesses the impact of climate change on wind-driven monetary losses caused by hurricanes in both present and future decades in NYC. Our approach involves several steps that we outline in the following sections:

#### 3.1 Downscaling of hurricanes and their corresponding wind events

In this section, we used the high-resolution statistical-deterministic tropical cyclone model to generate a large set of synthetic hurricanes, consistent with the ERA-Interim reanalysis and GCM climates, similar to the previous section. This approach allowed us to estimate the climatology and evolution of hurricanes' high-speed winds in the current and future decades in NYC. To represent the evolution of hurricanes under the SSP3 7.0 scenario, we used the large set of storms using three bias-corrected CMIP6 GCMs and the ERA-Interim reanalysis explained in the previous section. The downscaled surface maximum wind speed (with  $\sim 20$  m spatial resolution) during landfall of these synthetic hurricanes was used to quantify the associated monetary losses from wind hazard of hurricanes under the current and future warming climate.

#### 3.2 Optimizing damage function using conditional random field theory

The damage to properties caused by windstorms, such as hurricanes, increases rapidly with the wind speed. To model this relationship, we developed a damage function that expresses the fractional property losses as a function of the cube of the wind speed over a threshold value. The function also saturates at high wind speeds. We can represent this damage function mathematically as follows [34]:

$$f = \frac{v_n^3}{1 + v_n^3} \quad (1)$$

$$v_n = \frac{\max[(V - V_{\text{thresh}}), 0]}{V_{\text{half}} - V_{\text{thresh}}} \quad (2)$$

Here,  $f$  represents the fractional property value lost, and  $V$  is the surface maximum wind speed.  $V_{\text{thresh}}$  is the wind speed at or below which no damage occurs, and  $V_{\text{half}}$  is the wind speed at which half of the property value is lost. The damage function presented here is in line with previous studies that have used both theoretical and insurance claim data for damage calculations [35]. However, accurate quantification of damages and reduction of uncertainties in monetary losses for different building types and specific locations requires optimization of the damage function. This optimization can be achieved by tuning the parameters  $V_{\text{thresh}}$  and  $V_{\text{half}}$  using the Homesite wind damage claims and exposure database, which account for building codes and property strength in various coastal and inland regions.

To optimize the damage function, a grid-based approach with a spatial resolution of 5 km  $\times$  5 km is employed (Figure 6-A). Within each grid cell, historical hurricane maximum wind speeds are simulated using the physics-based model forced by re-analysis ERA5 data for Hurricanes Fay (2020), Henri (2021), Ida (2021), Isaias (2020), and Elsa (2021). The total fractional property losses to insured properties during the landfall of these hurricanes are calculated from the Homesite claim dataset. However, due to the limited number of available hurricane losses, it is not possible to extend the method to other historical hurricanes that occurred in the past. Therefore, to increase the number of samples and improve the optimization of the damage function in each grid cell, a physics-based augmentation technique is utilized. This technique generates multiple synthetic hurricanes for each historical hurricane, thereby increasing the number of wind samples per grid cell (Figure 6-A). In addition to generating multiple synthetic hurricanes, a small amount of noise is added to the damage part of each augmented historical hurricane to make the damages unique for each synthetic hurricane. By utilizing these augmented wind speed simulations and loss claims, the damage function is empirically derived for each grid cell. This empirically derived damage function includes a lower onset threshold and an upper damage threshold (Figure 6-B).

To improve the prediction of wind losses in each grid cell using equation 1, we developed an empirical function that incorporates information about wind speed and losses in each cell, as well as spatial information from surrounding grid cells, using the theory of conditional random fields (CRFs) [36]. The CRFs utilize unary and pairwise functions to model the relationship between wind speed and losses in each grid cell. The unary function captures the relationship between wind speed and losses in a given grid cell, while the pairwise function incorporates prior information from eight adjacent grid cells to account for the spatial correlation between wind speeds and losses (Figure 6-C). We describe the probability of a loss sequence in each grid cell given a maximum wind speed sequence using the following equation:

$$P(Y|X) = \frac{1}{Z} \exp \left( - \sum_{i=1}^m \lambda_i f_i(X, Y_c) \right) \quad (3)$$

$$Y_c = y_i x_i \quad \text{or} \quad Y_c = y_i y_j \quad (4)$$

The equation represents a conditional probability distribution, where  $Y$  represents the output variable (wind driven losses) and  $X$  represents the input variable (maximum wind speed). The model is based on the conditional random field (CRF) framework, which provides a way to model complex dependencies between these two variables. In this equation,  $Z$  is the normalization constant that ensures that the probabilities sum up to 1 over all possible values of  $Y$ . The  $\lambda_i$  are weights associated with each feature function  $f_i$ , which are defined over pairs of maximum wind speed and damage variables.

The feature functions capture the effect of wind speed ( $x_i$ ) on damage ( $y_i$ ), as well as the interaction between neighboring outputs ( $y_i$  and  $y_j$ ) on the probability of the current output (Figure 6-C). The term  $-\sum_{i=1}^m \lambda_i f_i(X, Y_c)$  represents the weighted sum of the feature functions over all pairs of maximum wind speed and damages in grid cells. The model assigns higher probabilities to damage sequences with lower energy, meaning sequences

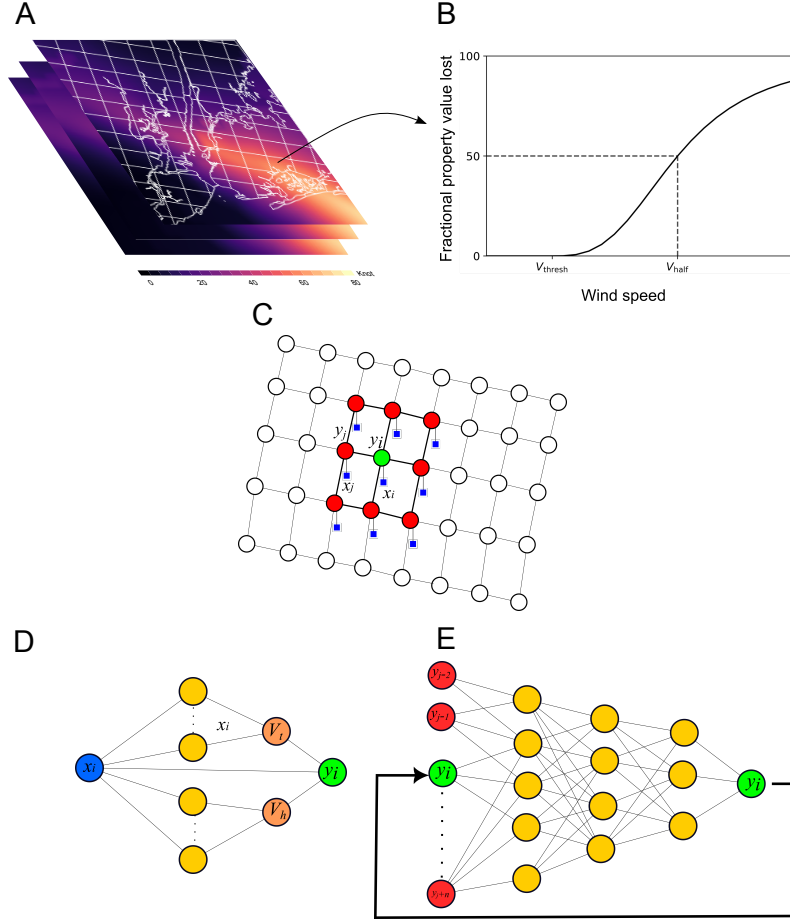


Figure 6: The process involves optimizing the damage function for each grid cell of size 5 km  $\times$  5 km. (A) augmenting the maximum surface wind speed from historical hurricanes, (B) creating an empirical model of the damage function that represents the relationship between maximum wind speed and fractional property value lost, (C) developing a Conditional Random Fields (CRFs) model to capture the relationship between wind speed and losses in each grid cell (unary function) and eight surrounding grid cell (pairwise function), (D) employing a simple neural network for the unary function to model the relationship between maximum wind speed and losses, to optimize the two wind thresholds ( $V_{\text{thresh}}$  and  $V_{\text{half}}$ ) in each target grid cell, and (E) using a Deep Learning model to learn the weights associated with each unary and pairwise feature function  $f_i$  in the CRF model.

that are more consistent with the maximum wind speed data. In other words, the model predicts the likelihood of different damages given a set of maximum wind speeds. Overall, this CRF model provides a powerful framework for modeling the complex relationships between wind speed and damages, which can have important applications in predicting monetary losses caused by severe weather events.

To accurately optimize the damage outputs in each grid cell, it is important to account for the complex relationship between wind speed and damages between different grid cells. To achieve this, we developed a deep learning model that learns the weights associated with each unary and pairwise feature function  $f_i$  in the CRF model. The deep learning model consists of input layers that represent the damage in the target grid cell and the eight surrounding cells, and an output layer that represents the predicted damage in the target cell (Figure 6, D and E). This structure is applied to all the grid cells

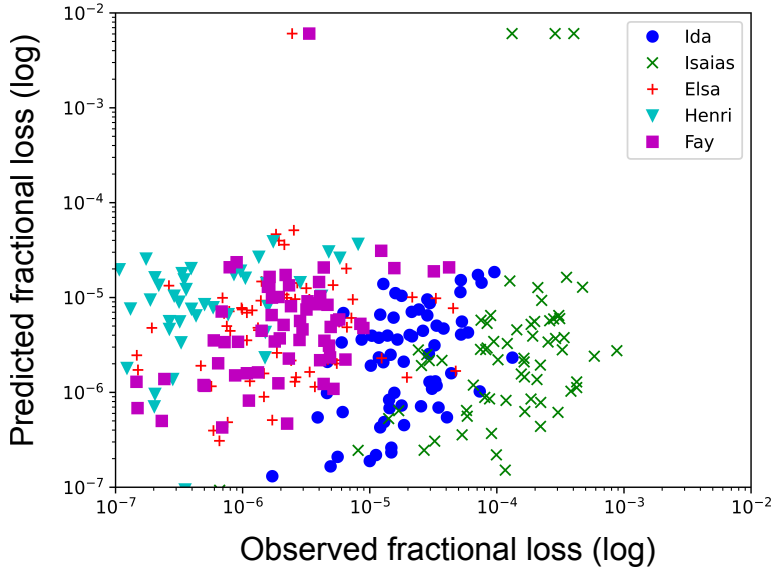


Figure 7: Evaluation of fractional property damage using Leave-One-Out process for the five observed hurricanes. (Results for each grid cell represented by dots).

in the study area simultaneously to train the  $\lambda_i$  weights associated with each feature function  $f_i$ . The number of hidden layers, neurons, and activation functions for each layer are specified. To train the model, we used a stochastic gradient descent optimization algorithm that minimizes the loss function between predicted and actual damage in each grid cell simultaneously. The weights of the model are updated iteratively to improve prediction accuracy.

This deep learning model provides an effective approach to capture the intricate relationship between wind speed and damages among neighboring grid cells within the study area. By adjusting the weights assigned to each feature function  $f_i$ , we can precisely optimize the two thresholds outlined in equation 2 and subsequently the damage function for each grid cell. The optimized damage function has the potential to predict monetary losses resulting from future hurricanes.

The performance of our model was assessed using leave-one-out cross-validation to evaluate its performance on five historical hurricanes. The results of this evaluation are presented in Figure 7, which shows the model’s performance on each of the five historical hurricanes. We found that the model was effective in capturing the complex relationships between wind speed and damages, and its predicted fractional damages were aligned with the observed damages from each hurricane. Figure 7 illustrates these findings by demonstrating that the model effectively modeled the complex relationships between wind speed and damages. These results provide evidence that our model can accurately predict wind-driven financial losses caused by hurricanes.

Figure 8 shows the optimized damage function for each grid cell in our study area. We found that integrating spatial information through Conditional Random Fields (CRFs) improves the accuracy of predicting wind-driven financial losses when compared to conventional techniques. These optimized damage functions were specifically tailored to the insured portfolio of Homesite in this study area. We then utilized these optimized

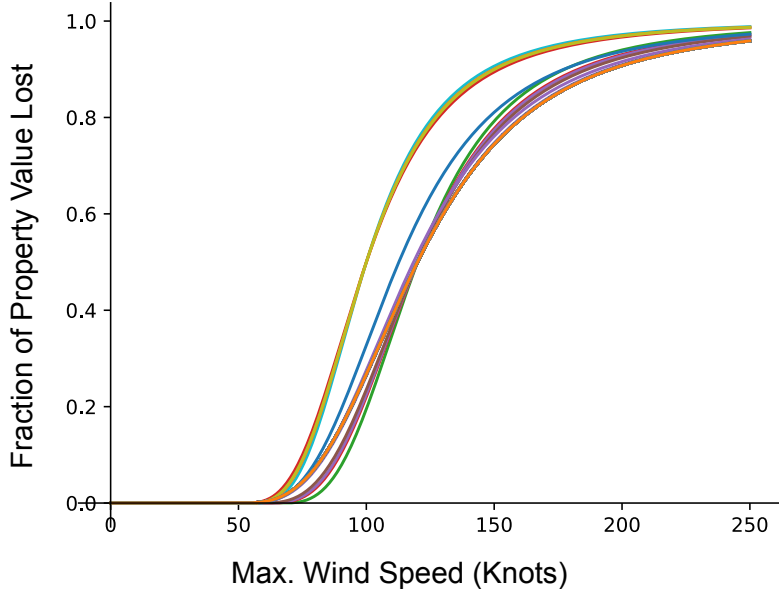


Figure 8: Optimized damage functions for each grid cell in the study area

functions and pair-wise CRF functions to quantify the monetary losses from wind-driven damages that may arise from future intensifying hurricanes in the coming decades. To achieve this, we employed the physics-based model to simulate a large set of synthetic hurricanes that are projected to pass through NYC by the middle and end of the century. These simulations were obtained from the three CMIP6 climate models under the SSP3-7.0 scenario.

By replacing the maximum wind speed of these synthetic hurricanes in the optimized damage functions, we can calculate the monetary losses that may arise from each hurricane in each specific grid cell. Summing up the total monetary losses for the entire area enables us to generate a large set of monetary losses from different weak and strong hurricanes in the past, current, and future decades. These total monetary losses are then used to assess the risk of monetary losses caused by hurricanes' strong winds under a warming climate in the future decades.

### 3.3 Quantifying the risk of monetary losses from intensifying storms in current and future climates

To assess the potential impact of future intensifying storms on monetary losses, we utilized optimized damage functions that were tailored to each grid cell. By incorporating the maximum wind speed projections from downscaled future storms into these damage functions, we calculated the fractional damages to insured properties. This approach enables us to generate a large dataset of fractional property value losses that can be multiplied by the total property values to estimate the property monetary losses resulting from the past, current, and future storms. This methodology allows for a more comprehensive and accurate assessment of the potential economic impacts of intensified storms in the future.

To assess the potential increase in the risk of monetary losses resulting from intensifying

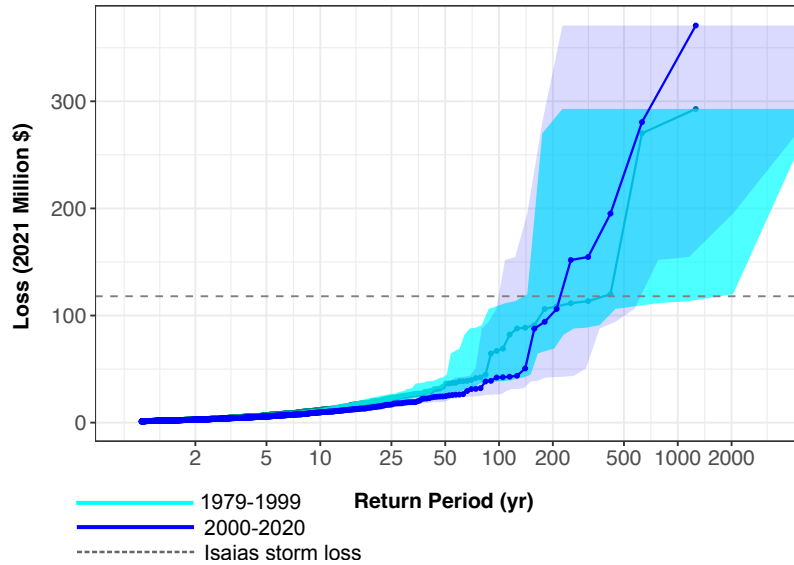


Figure 9: Monetary Loss Risk from Wind Damage of Hurricanes to Homesite Insured Properties in the Late 20th Century and Current Climate based on ERA5 Reanalysis Data: Uncertainty Bounds Calculated using 5th and 95th Percentiles of a Poisson Distribution

storms due to climate change, we employed a probabilistic analysis across different return periods in past, current and future decades. The return periods are calculated based on annual exceedance probability. We account for the inherent uncertainty in the monetary losses by utilizing multiple climate model simulations and sampling uncertainty for low and high frequency storms.

Figure 9 displays the monetary losses associated with hurricanes in the late 20th century and the current climate, as a function of different return periods. Each dot on the plot represents the monetary losses for Homesite insured properties from each hurricane in the two time periods in the study area. The loss results are probabilistic and indicate the likelihood of such losses occurring. For instance, storms similar to Hurricane Isaias (which caused a monetary loss of \$117 million) would be expected to occur once every  $\sim 400$  yr years in the late 20th century and every  $\sim 200$  yr years in the current climate, indicating a doubling of the risk of monetary losses for such a hurricane in the current climate. This translates to a probability of such a monetary loss occurring from such a hurricane every year of 0.25 percent in the late 20th century and 0.5 percent every year in the current climate. The same presented values of monetary losses correspond to different likelihoods of occurrence in the late 20th century and current climates. For instance, the monetary losses with a likelihood of 2% in each given year amount to \$24 million, while the losses with a likelihood of 1% are valued at \$42 million in the current climate. Similarly, the losses with a likelihood of 0.5% amount to \$106 million, and those with a likelihood of 0.1% are valued at \$340 million. These values indicate the increasing probability of higher monetary losses associated with lower likelihoods of occurrence.

Figure 10 presented here shows the monetary losses caused by wind damage from hurricanes in the study area for three different time periods - current, mid-century and end of century. The risk of monetary losses is also quantified in a probabilistic manner and is presented as a function of return periods.

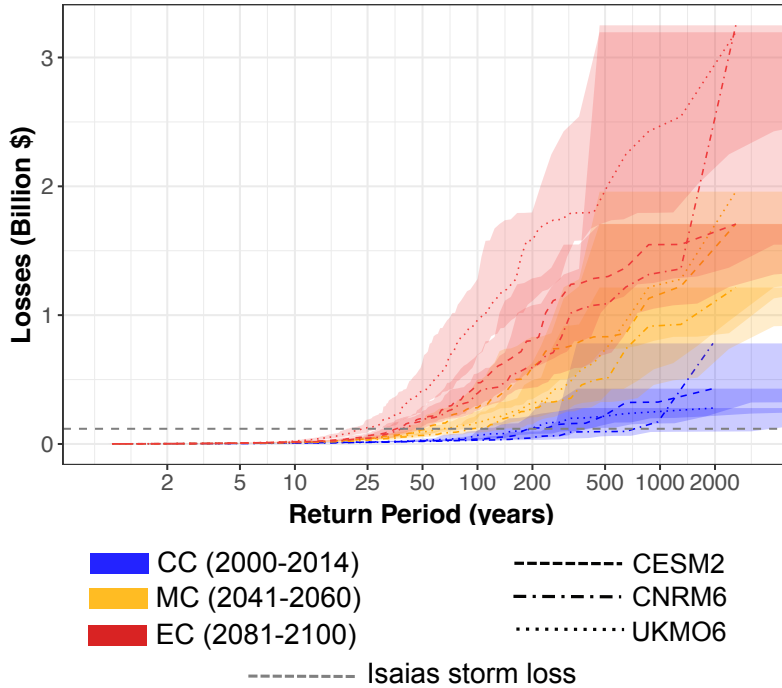


Figure 10: Monetary Loss Risk from Wind Damage of Hurricanes to Homesite Insured Properties in current and future decades from three climate model simulations. Uncertainty Bounds Calculated using 5th and 95th Percentiles of a Poisson Distribution

For example, the ensemble mean of monetary losses that occur once every 100 years or with a probability of 1% in each given year in the current climate is approximately \$45 million. This value increases to \$190 million by the mid-century and \$610 million by the end of century. This implies that the risk of monetary losses for such storms will increase up to 4 times by the mid-century and 13.5 times by the end of century. Another way to interpret the monetary risk results is by quantifying the return period or likelihood of occurrence for a specific monetary loss. For instance, the frequency of monetary losses similar to those caused by extreme storms like Isaias (valued at \$117 million) in the study area based on ensemble mean of the three climate models is once every  $\sim 350$  *yr* in the current climate, once every  $\sim 70$  *yr* years by the mid-century, and once every  $\sim 30$  *yr* years by the end of century. This means that the likelihood of occurrence for such a monetary loss from an Isaias-like storm for each given year in the current climate is 0.29%, and it increases to 1.4% by the mid-century and 3.3% by the end of century. Similarly, the likelihood of occurrence for other high frequency and low frequency wind-driven monetary losses from hurricanes can also be estimated for the study area. The results demonstrate that climate change increases the monetary losses from wind-driven damage resulting from hurricanes in the study area.

### 3.4 Discussion

Our study showed that incorporating physics-based methodology can significantly improve the accuracy of predictions of wind-driven monetary losses caused by hurricanes. By integrating a range of factors, including wind speed, losses during landfalling of historical hurricanes, and spatial information from surrounding cells, our empirical damage functions have provided a robust foundation for accurate predictions. Furthermore, the

use of conditional random field and deep learning models enabled us to capture the complex relationship between wind speed and damages, making our model highly effective in predicting monetary losses to Homesite insured properties given a set of maximum wind speeds from future intensifying storms under the impact of climate change.

Our findings have significant implications for the insurance industry and emergency management agencies. Accurate predictions of monetary losses resulting from hurricanes can inform pricing strategies, enabling insurers to prepare for future intensifying losses from these storms. Additionally, the methodology we have developed can be extended to vulnerable areas in the U.S., providing valuable insights into the locations that are most vulnerable to monetary losses from intensifying storms and their potential increase in vulnerability in the future under the effect of climate change.

As an insurance company, Homesite can leverage these results to develop new policies, set premiums, and respond to claims related to the hazards from these intensifying storms in a future warming climate. Overall, our study provides a powerful tool for predicting wind-driven financial losses caused by hurricanes, and we believe that it has the potential to make a significant impact in the field of risk management, as well as contribute to our understanding of the effects of climate change on extreme weather events.

## 4 Publications supported under this contract

Here is the list of publications supported for this research contract:

- Sarhadi Ali, Raphae l Rousseau-Rizzi, Kyle Mandli, Jeffrey Neal, Michael P. Wiper, Monika Feldmann, and Kerry Emanuel, 2023, “Contributions to increasing compound flooding risk in New York City”, **Bulletin of the American Meteorological Society**, Under Review.

In addition, the results of this research were presented at different conferences. Here is the list of presentations:

- Sarhadi, A., Kerry Emanuel, 2022, “Climate change is increasing the risk of compound flooding by tropical cyclones in New York City”, American Geophysical Union (AGU), Chicago.
- Sarhadi, A., Kerry Emanuel, 2022, “Future risk of compound flooding from Tropical Cyclones”, Symposium on Hurricane Risk in a Changing Climate, Florida.
- Sarhadi, A., Kerry Emanuel, 2022, “Compound Flooding Risk from Tropical Cyclones Under A Warming Climate”, American Meteorological Society (AMS) 102nd Annual Meeting, Houston, Texas.
- Sarhadi, A., Kerry Emanuel, 2021, “Tropical Cyclone Rainfall-driven Flooding Risk Under A Warming Climate”, The AMS 34th Conference on Hurricanes and Tropical Meteorology Virtual Meeting.

- Sarhadi, A., Kerry Emanuel, 2021, “Inland Coastal Flooding Risk by Tropical Cyclone”, European Geosciences Union (EGU) General Assembly, Vienna, Austria.
- Sarhadi, A., Kerry Emanuel, 2021, “Tropical Cyclone Rainfall-driven Flood Risk Assessment”, NRC 6th Annual Probabilistic Flood Hazard Assessment Workshop.

## References

- [1] L. A. Bakkensen and R. O. Mendelsohn, “Global tropical cyclone damages and fatalities under climate change: An updated assessment,” *Hurricane risk*, pp. 179–197, 2019.
- [2] A. B. Smith *et al.*, “Us billion-dollar weather and climate disasters, 1980–present (ncei accession 0209268),” *NOAA National Centers for Environmental Information*, vol. 10, 2020.
- [3] W. Zhang, G. Villarini, G. A. Vecchi, and J. A. Smith, “Urbanization exacerbated the rainfall and flooding caused by hurricane harvey in houston,” *Nature*, vol. 563, no. 7731, pp. 384–388, 2018.
- [4] E. N. Rappaport, “Fatalities in the united states from atlantic tropical cyclones: New data and interpretation,” *Bulletin of the American Meteorological Society*, vol. 95, no. 3, pp. 341–346, 2014.
- [5] B. H. Strauss, P. M. Orton, K. Bittermann, M. K. Buchanan, D. M. Gilford, R. E. Kopp, S. Kulp, C. Massey, H. d. Moel, and S. Vinogradov, “Economic damages from hurricane sandy attributable to sea level rise caused by anthropogenic climate change,” *Nature communications*, vol. 12, no. 1, pp. 1–9, 2021.
- [6] C. M. Patricola and M. F. Wehner, “Anthropogenic influences on major tropical cyclone events,” *Nature*, vol. 563, no. 7731, pp. 339–346, 2018.
- [7] T. Wahl, S. Jain, J. Bender, S. D. Meyers, and M. E. Luther, “Increasing risk of compound flooding from storm surge and rainfall for major us cities,” *Nature Climate Change*, vol. 5, no. 12, pp. 1093–1097, 2015.
- [8] K. Emanuel, “Response of global tropical cyclone activity to increasing co<sub>2</sub>: Results from downscaling cmip6 models,” *Journal of Climate*, vol. 34, no. 1, pp. 57–70, 2021.
- [9] M. A. Bender, T. R. Knutson, R. E. Tuleya, J. J. Sirutis, G. A. Vecchi, S. T. Garner, and I. M. Held, “Modeled impact of anthropogenic warming on the frequency of intense atlantic hurricanes,” *Science*, vol. 327, no. 5964, pp. 454–458, 2010.
- [10] K. Emanuel, “Increasing destructiveness of tropical cyclones over the past 30 years,” *Nature*, vol. 436, no. 7051, pp. 686–688, 2005.
- [11] —, “Atlantic tropical cyclones downscaled from climate reanalyses show increasing activity over past 150 years,” *Nature communications*, vol. 12, no. 1, pp. 1–8, 2021.
- [12] K. A. Emanuel, “Downscaling cmip5 climate models shows increased tropical cyclone activity over the 21st century,” *Proceedings of the National Academy of Sciences*, vol. 110, no. 30, pp. 12 219–12 224, 2013.
- [13] K. E. Trenberth, L. Cheng, P. Jacobs, Y. Zhang, and J. Fasullo, “Hurricane harvey

- links to ocean heat content and climate change adaptation,” *Earth’s Future*, vol. 6, no. 5, pp. 730–744, 2018.
- [14] M. A. Saunders and A. S. Lea, “Large contribution of sea surface warming to recent increase in atlantic hurricane activity,” *Nature*, vol. 451, no. 7178, pp. 557–560, 2008.
- [15] P. Huang, I.-I. Lin, C. Chou, and R.-H. Huang, “Change in ocean subsurface environment to suppress tropical cyclone intensification under global warming,” *Nature Communications*, vol. 6, no. 1, pp. 1–9, 2015.
- [16] K. J. Walsh, S. J. Camargo, G. A. Vecchi, A. S. Daloz, J. Elsner, K. Emanuel, M. Horn, Y.-K. Lim, M. Roberts, C. Patricola *et al.*, “Hurricanes and climate: The us clivar working group on hurricanes,” *Bulletin of the American Meteorological Society*, vol. 96, no. 6, pp. 997–1017, 2015.
- [17] M. D. Priestley and J. L. Catto, “Future changes in the extratropical storm tracks and cyclone intensity, wind speed, and structure,” *Weather and Climate Dynamics*, vol. 3, no. 1, pp. 337–360, 2022.
- [18] J. P. Kossin, K. A. Emanuel, and G. A. Vecchi, “The poleward migration of the location of tropical cyclone maximum intensity,” *Nature*, vol. 509, no. 7500, pp. 349–352, 2014.
- [19] J. F. Booth, V. Narinesingh, K. L. Towey, and J. Jeyaratnam, “Storm surge, blocking, and cyclones: A compound hazards analysis for the northeast united states,” *Journal of Applied Meteorology and Climatology*, vol. 60, no. 11, pp. 1531–1544, 2021.
- [20] A. Gori, N. Lin, D. Xi, and K. Emanuel, “Tropical cyclone climatology change greatly exacerbates us joint rainfall-surge hazard,” 2021.
- [21] A. J. Garner, M. E. Mann, K. A. Emanuel, R. E. Kopp, N. Lin, R. B. Alley, B. P. Horton, R. M. DeConto, J. P. Donnelly, and D. Pollard, “Impact of climate change on new york city’s coastal flood hazard: Increasing flood heights from the preindustrial to 2300 ce,” *Proceedings of the National Academy of Sciences*, vol. 114, no. 45, pp. 11 861–11 866, 2017.
- [22] A. J. Reed, M. E. Mann, K. A. Emanuel, N. Lin, B. P. Horton, A. C. Kemp, and J. P. Donnelly, “Increased threat of tropical cyclones and coastal flooding to new york city during the anthropogenic era,” *Proceedings of the National Academy of Sciences*, vol. 112, no. 41, pp. 12 610–12 615, 2015.
- [23] K. Emanuel, “Assessing the present and future probability of hurricane harvey’s rainfall,” *Proceedings of the National Academy of Sciences*, vol. 114, no. 48, pp. 12 681–12 684, 2017.
- [24] N. Lin, R. E. Kopp, B. P. Horton, and J. P. Donnelly, “Hurricane sandy’s flood frequency increasing from year 1800 to 2100,” *Proceedings of the National Academy of Sciences*, vol. 113, no. 43, pp. 12 071–12 075, 2016.

- [25] R. Marsooli, N. Lin, K. Emanuel, and K. Feng, “Climate change exacerbates hurricane flood hazards along us atlantic and gulf coasts in spatially varying patterns,” *Nature communications*, vol. 10, no. 1, pp. 1–9, 2019.
- [26] A. Gori, N. Lin, D. Xi, and K. Emanuel, “Tropical cyclone climatology change greatly exacerbates us extreme rainfall–surge hazard,” *Nature Climate Change*, vol. 12, no. 2, pp. 171–178, 2022.
- [27] P. D. Bates, N. Quinn, C. Sampson, A. Smith, O. Wing, J. Sosa, J. Savage, G. Olcese, J. Neal, G. Schumann *et al.*, “Combined modeling of us fluvial, pluvial, and coastal flood hazard under current and future climates,” *Water Resources Research*, vol. 57, no. 2, p. e2020WR028673, 2021.
- [28] K. Emanuel, R. Sundararajan, and J. Williams, “Hurricanes and global warming: Results from downscaling ipcc ar4 simulations,” *Bulletin of the American Meteorological Society*, vol. 89, no. 3, pp. 347–368, 2008.
- [29] M. Feldmann, K. Emanuel, L. Zhu, and U. Lohmann, “Estimation of atlantic tropical cyclone rainfall frequency in the united states,” *Journal of Applied Meteorology and Climatology*, vol. 58, no. 8, pp. 1853–1866, 2019.
- [30] M. Komurcu, K. Emanuel, M. Huber, and R. Acosta, “High-resolution climate projections for the northeastern united states using dynamical downscaling at convection-permitting scales,” *Earth and Space Science*, vol. 5, no. 11, pp. 801–826, 2018.
- [31] K. T. Mandli and C. N. Dawson, “Adaptive mesh refinement for storm surge,” *Ocean Modelling*, vol. 75, pp. 36–50, 2014.
- [32] J. Neal, G. Schumann, and P. Bates, “A subgrid channel model for simulating river hydraulics and floodplain inundation over large and data sparse areas,” *Water Resources Research*, vol. 48, no. 11, 2012.
- [33] N. Lin, K. Emanuel, M. Oppenheimer, and E. Vanmarcke, “Physically based assessment of hurricane surge threat under climate change,” *Nature Climate Change*, vol. 2, no. 6, pp. 462–467, 2012.
- [34] K. Emanuel, “Global warming effects on us hurricane damage,” *Weather, Climate, and Society*, vol. 3, no. 4, pp. 261–268, 2011.
- [35] C. C. Watson Jr and M. E. Johnson, “Hurricane loss estimation models: Opportunities for improving the state of the art,” *Bulletin of the American Meteorological Society*, vol. 85, no. 11, pp. 1713–1726, 2004.
- [36] C. Sutton, A. McCallum *et al.*, “An introduction to conditional random fields,” *Foundations and Trends® in Machine Learning*, vol. 4, no. 4, pp. 267–373, 2012.

# A Appendix

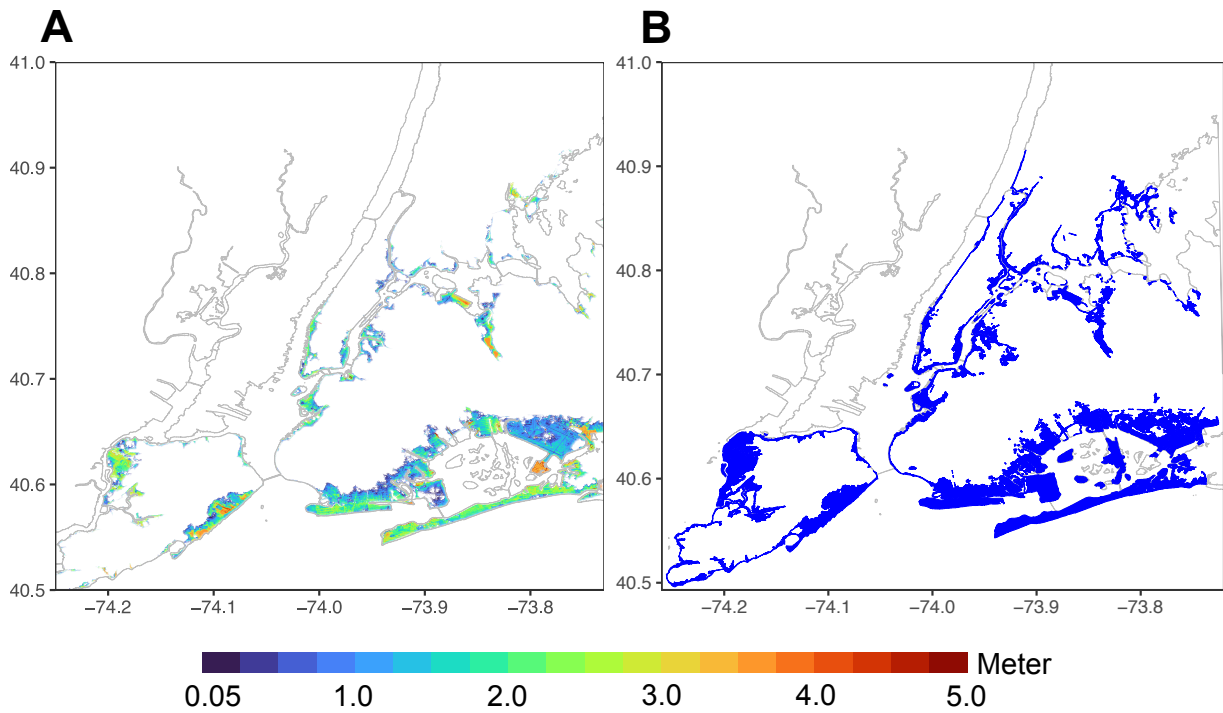


Figure 1: Performance evaluation of the LISFLOOD hydraulic model in simulating Sandy's surge driven flooding occurred in October 2012 in NYC. (A) Simulated surge driven flooding map from the Sandy-like event (synthetic track 1299 downscaled from ERA-Interim reanalysis) restricted to NYC. (B) Sandy's surge driven flooding extent map recorded from FEMA in NYC. Note that the FEMA map does not show flood levels but only areas inundated. The FEMA flood inundation map is downloadable from: <https://data.cityofnewyork.us/Environment/Sandy-Inundation-Zone/uyj8-7rv5>

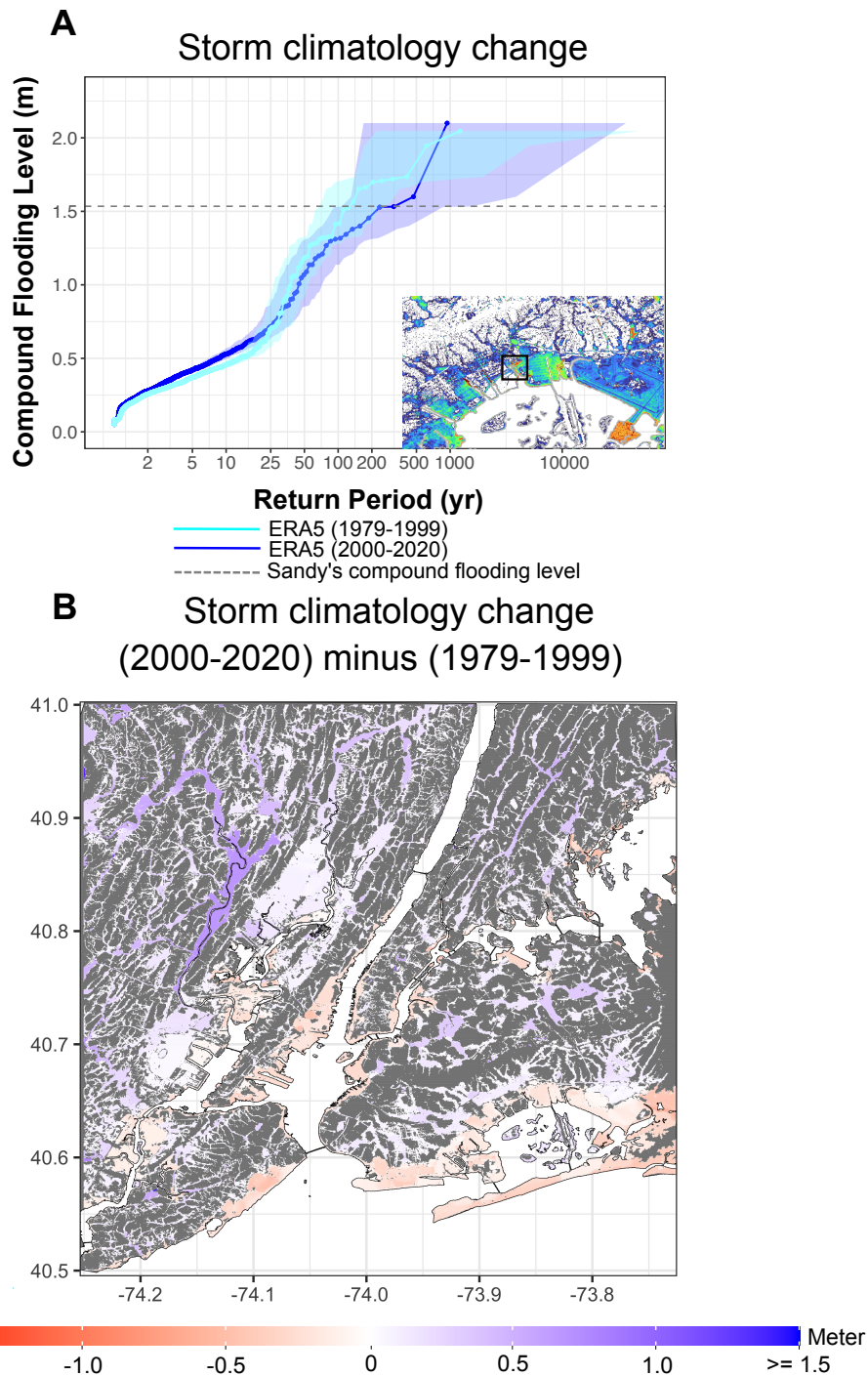


Figure 2: Impact of only TC climatology changes on the risk of compound flooding in today's climate (2000-2020) relative to the end of the 20<sup>th</sup> century (1979-1999) in NYC. (A) TC compound flooding level as a function of return period for today's climate and the end of the 20<sup>th</sup> century (the results are calculated based on the mean of compound flooding for the depicted area). Each line shows compound flooding results from synthetic TCs generated from ERA-Interim reanalyses over each time period. The gray dashed line shows the mean of Sandy compound flooding level calculated from the Sandy-like event (#1299) for the depicted area (shown in a black rectangle). (B) Impact of only TC climatology changes on the spatial risk of 100 *y* return period compound flooding events in today's climate relative to the 20<sup>th</sup> century (blue color shows increasing trend, and red color shows decreasing trend).

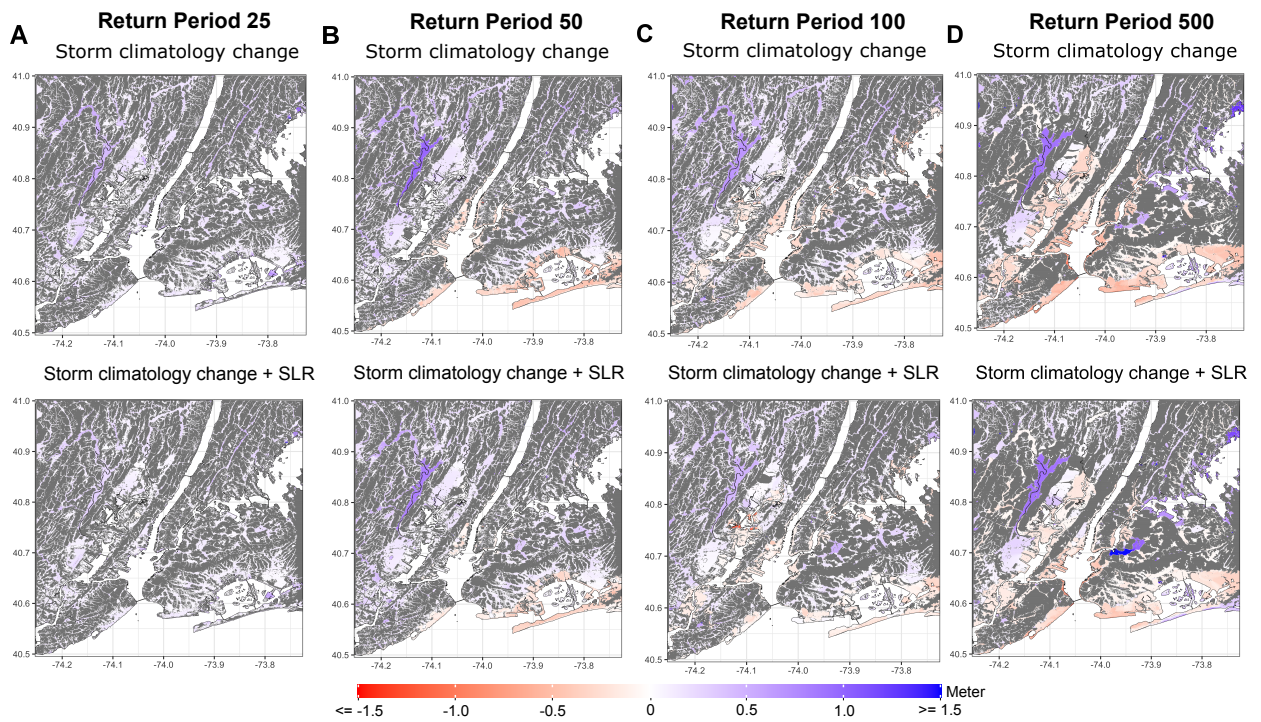


Figure 3: (A-D) Individual and joint contribution of storm climatology changes and SLR on the spatial risk of TC compound flooding events in today's climate (2000-2020) relative to the late 20<sup>th</sup> century (1979-1999) at different return periods. Blue color represents increasing trend, and red color represents decreasing trend.

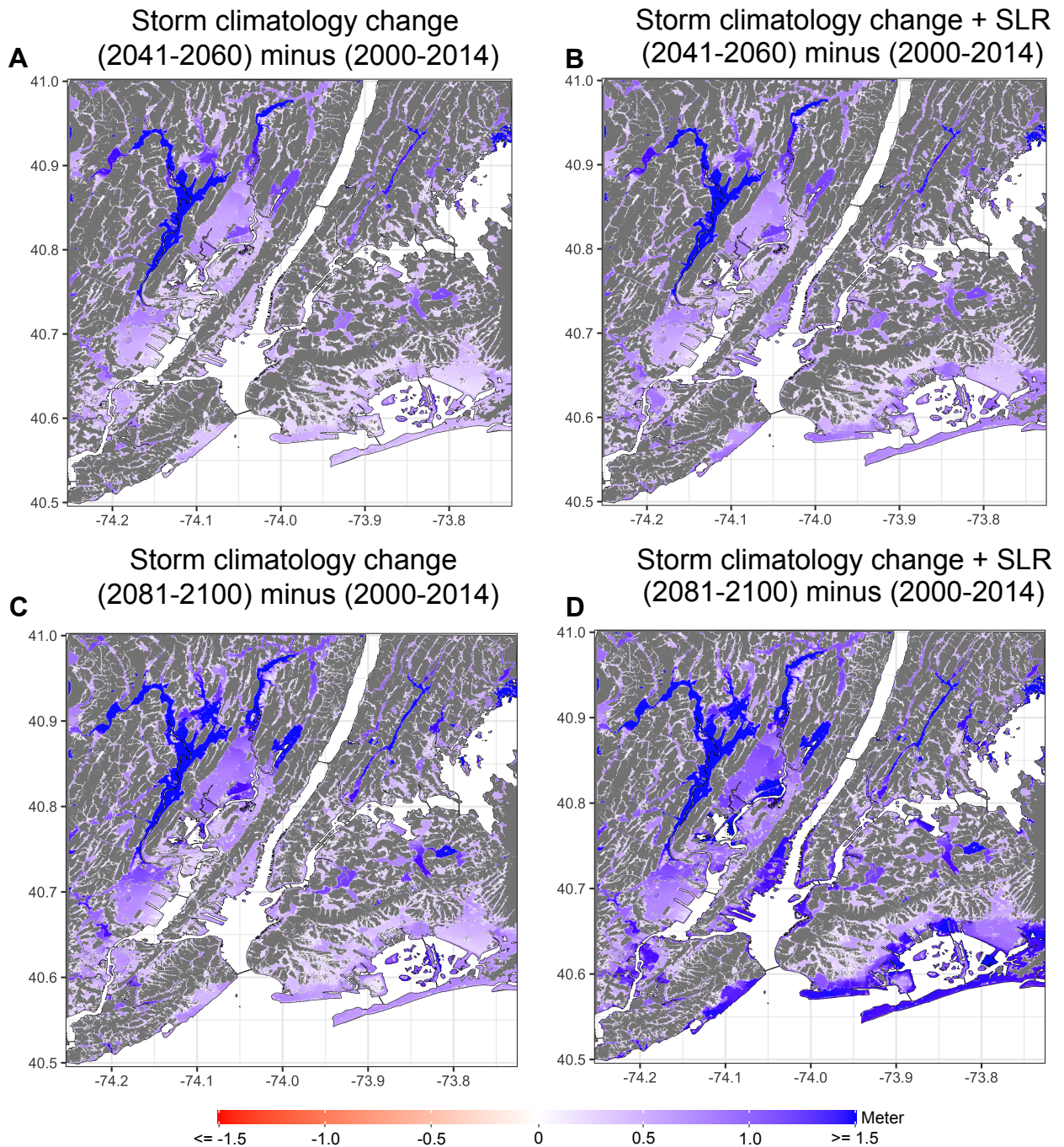


Figure 4: (A and B) Impact of storm climatology changes on the spatial risk of 50  $y$  return period TC compound flooding events by the middle of the century relative to the current climate (upper left) and by the end of the century relative to the current climate (upper right). (C and D) Impact of storm climatology changes and SLR on the spatial risk of 50  $y$  return period TC compound flooding events by the middle of the century relative to the current climate (lower left) and by the end of the century relative to the current climate (lower right).

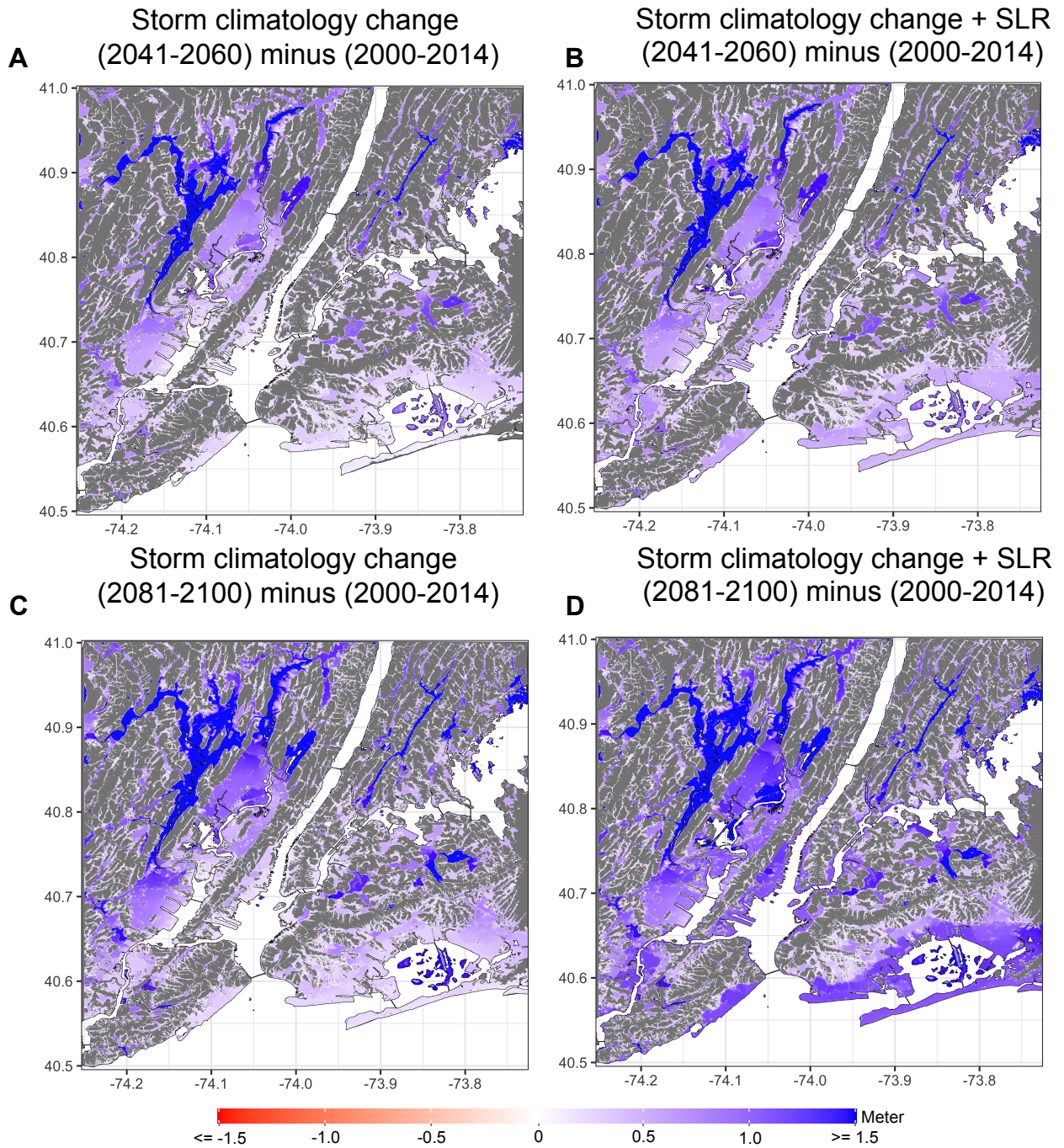


Figure 5: Similar to Fig. S4, but for 100  $y$  return period.

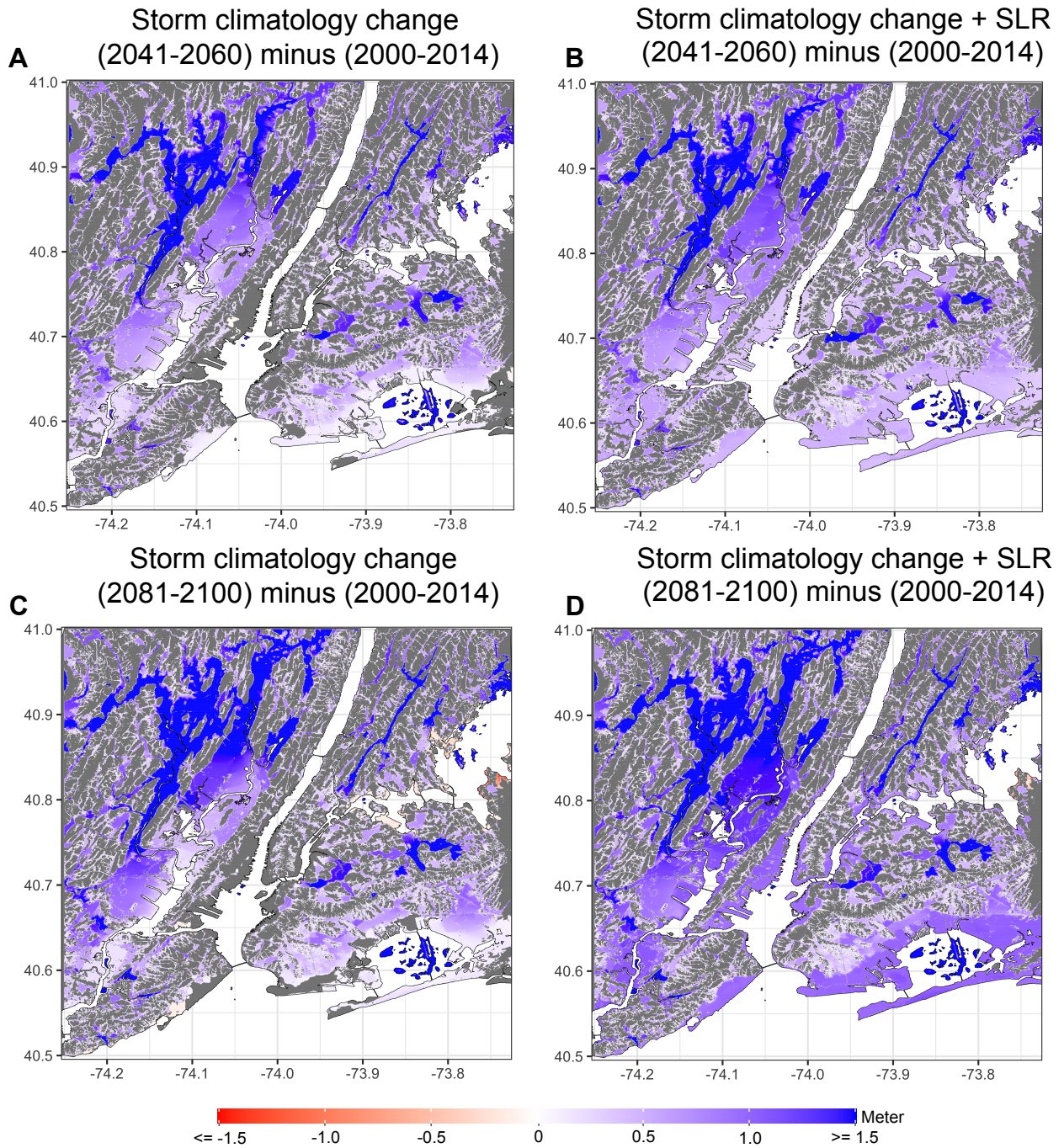


Figure 6: Similar to Fig. S4, but for 500  $y$  return period.

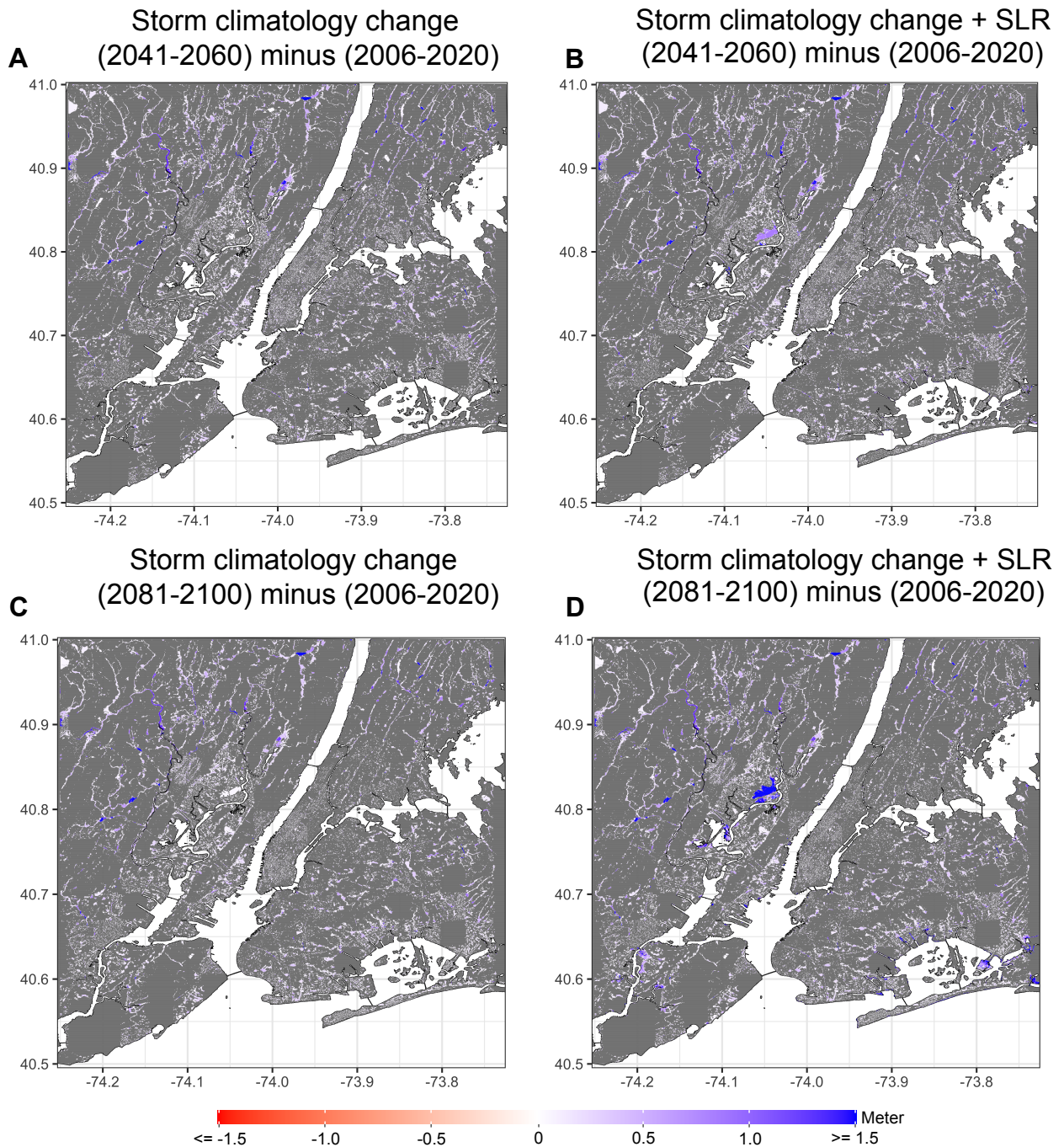


Figure 7: (A and B) Impact of storm climatology changes on the spatial risk of 5 *y* return period ETC compound flooding events by the middle of the century relative to the current climate (upper left) and by the end of the century relative to the current climate (upper right). (C and D) Impact of storm climatology changes and SLR on the spatial risk of 5 *y* return period ETC compound flooding events by the middle of the century relative to the current climate (lower left) and by the end of the century relative to the current climate (lower right).

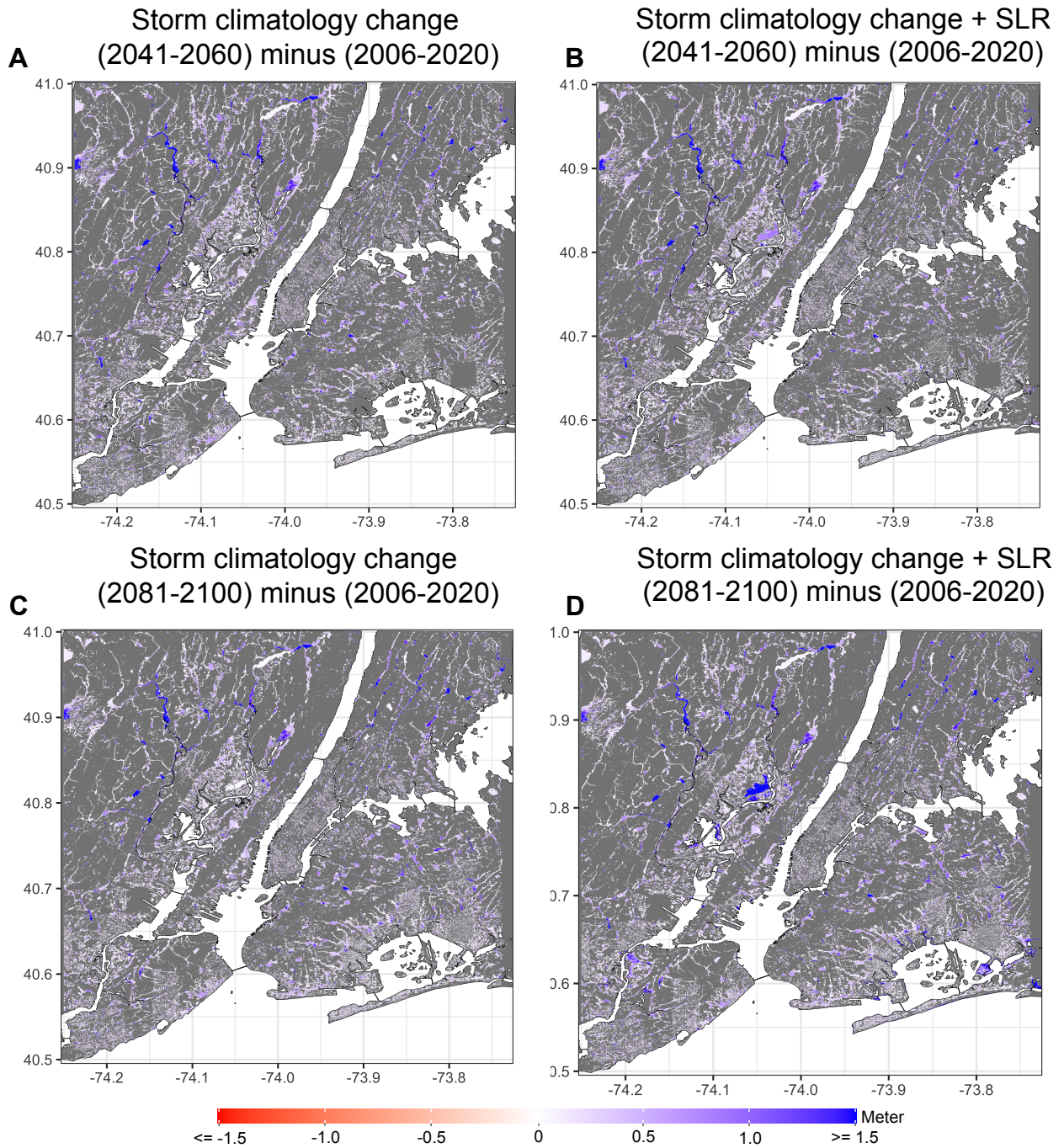


Figure 8: Similar to Fig. S8, but for 10  $y$  return period.

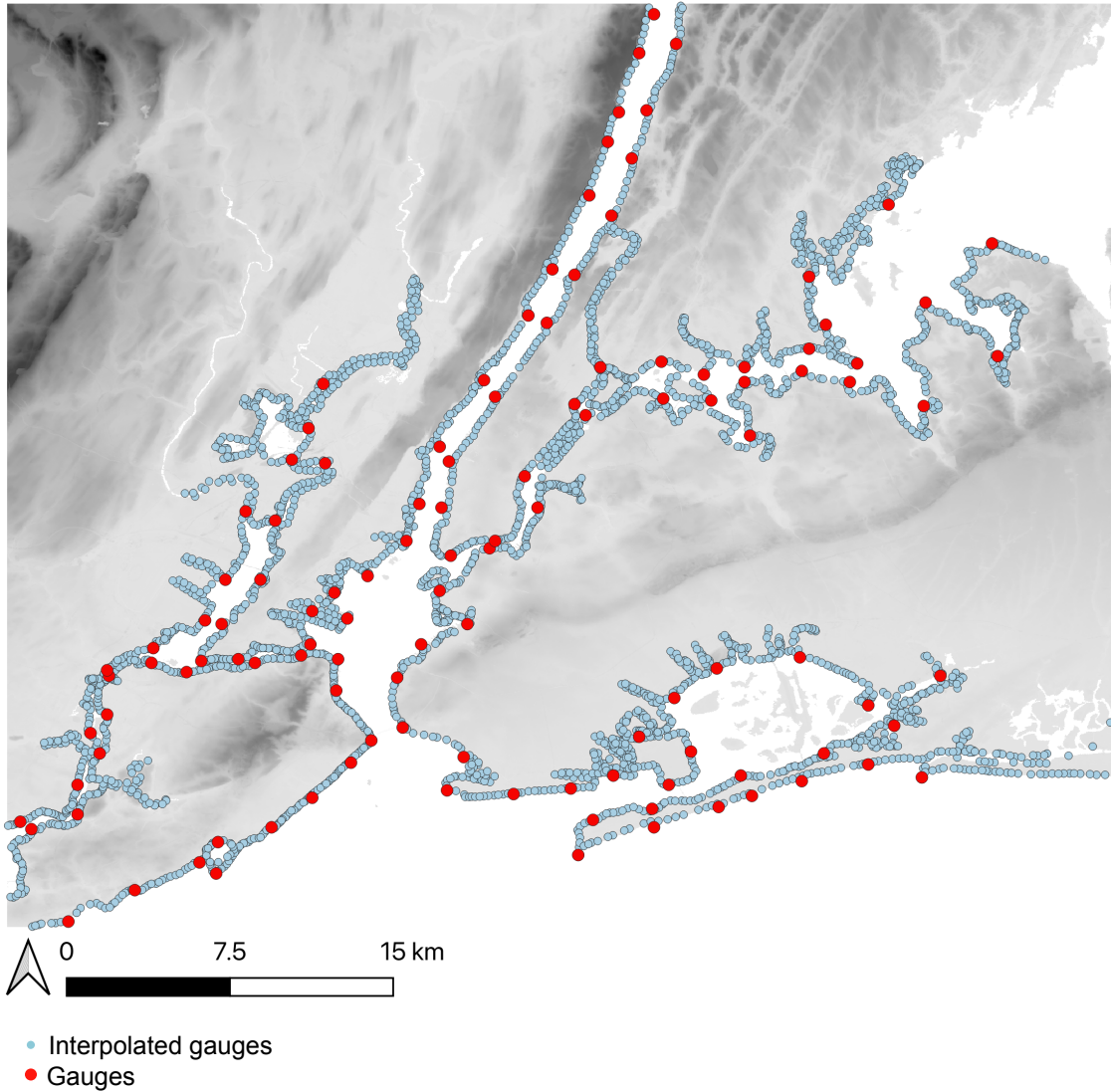


Figure 9: Location of synthetic gauges used for surge modeling of TC and ETC storms in NYC. Red points show the location of the main synthetic gauges (118 gauges) assigned across the coastline to record simulated surge heights by GeoCLAW. Blue points show the location of interpolated synthetic gauges (3113 gauges) assigned between the main synthetic gauges to cover the entire coastline.

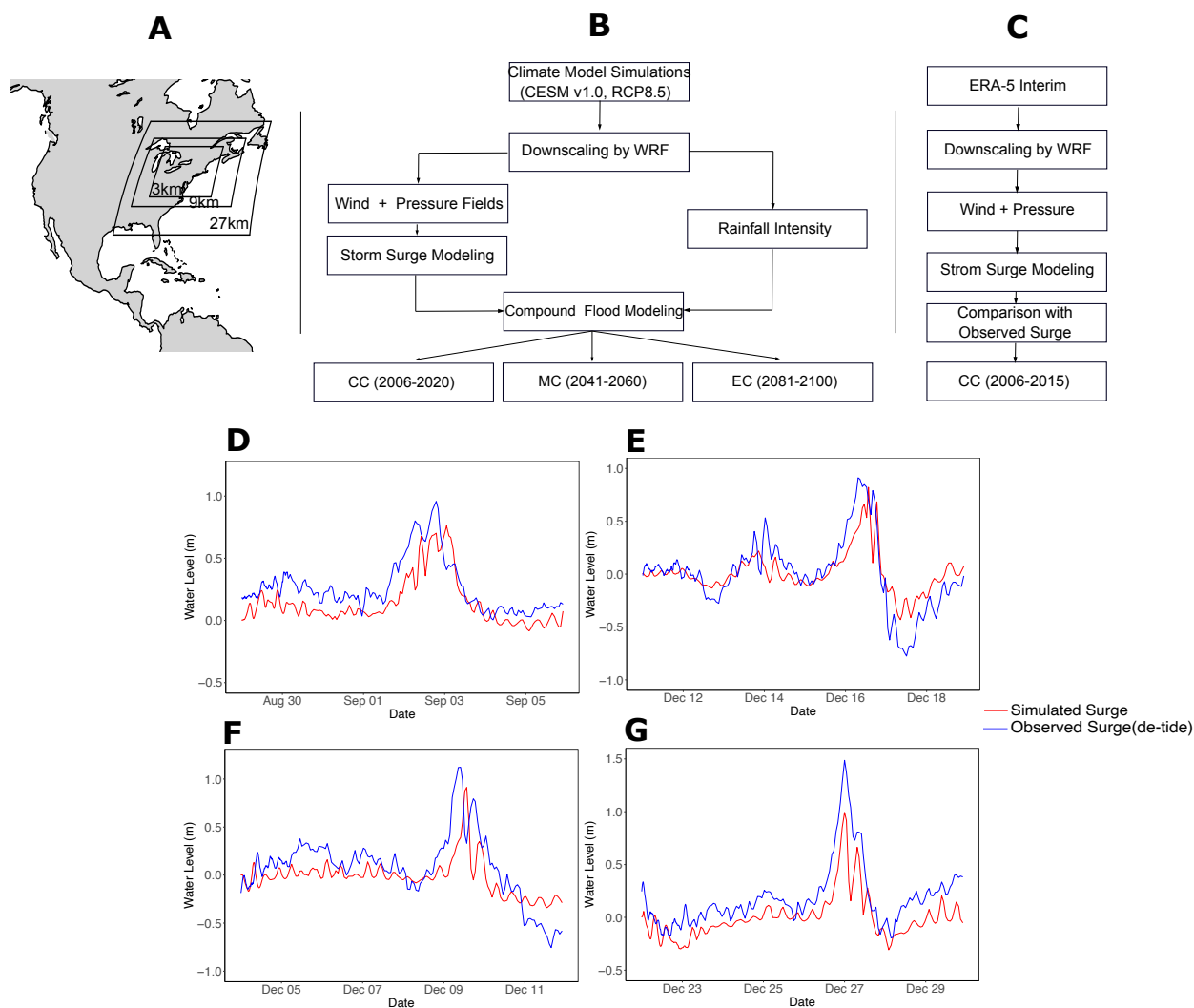


Figure 10: Process of downscaling and compound flood modeling from ETCs in historical and future climates. (A) Three nested grids of 27, 9, and 3-km spatial resolution used for dynamically downscaling WRF simulations (in this study we use downscaled WRF simulations of wind and rainfall within the 3-km spatial resolution domain). (B) Process of ETCs compound flood modeling in the current and future climates. (C) Evaluation process of surge modeling based on historical ETCs downscaled by WRF simulations driven by ERA-Interim reanalyses in the current climate. (D-G) Performance evaluation of GeoCLAW for historical ETC storms, which occurred in August 2006 (upper left), December 2007 (upper right), December 2009 (lower left), and December 2012 (lower right). Blue line represents observed surge heights during landfalling of the ETCs, calculated by de-tiding water levels (water elevation is subtracted from NOAA tide prediction at the Battery gauge). Red line represents surge heights simulated by GeoCLAW from WRF downscaled hourly wind and pressure fields driven by ERA-Interim reanalysis for the same historical events. Note that the temporal resolution in the x-axis is six minutes.